J. Fluid Mech. (1993), *vol.* 250, *pp.* 169–207

A mechanism for bypass transition from localized disturbances in wall-bounded shear flows

By DAN S. HENNINGSON[1]†, ANDERS LUNDBLADH[2]† AND ARNE V. JOHANSSON[2]

[1] Department of Mathematics, Massachusetts Institute of Technology, Cambridge, MA 02139, USA

[2] Department of Mechanics, Royal Institute of Technology, S-10044 Stockholm, Sweden

(Received 3 October 1991 and in revised form 16 November 1992)

The linear, nonlinear and breakdown stages in the transition of localized disturbances in plane Poiseuille flow is studied by direct numerical simulations and analysis of the linearized Navier–Stokes equations. Three-dimensionality plays a key role and allows for algebraic growth of the normal vorticity through the linear *lift-up* mechanism. This growth primarily generates elongated structures in the streamwise direction since it is largest at low streamwise wavenumbers. For finite-amplitude disturbances such structures will be generated essentially independent of the details of the initial disturbance, since the preferred nonlinear interactions transfer energy to low streamwise wavenumbers. The nonlinear interactions also give a decrease in the spanwise scales. For the stronger initial disturbances the streamwise vorticity associated with the slightly inclined streaks was found to roll up into distinct streamwise vortices in the vicinity of which breakdown occurred. The breakdown starts with a local rapid growth of the normal velocity bringing low-speed fluid out from the wall. This phenomenon is similar to the low-velocity spikes previously observed in transition experiments. Soon thereafter a small turbulent spot is formed. This scenario represents a *bypass* of the regular Tollmien–Schlichting, secondary instability process. The simulations have been carried out with a sufficient spatial resolution to ensure an accurate description of all stages of the breakdown and spot formation processes. The generality of the observed processes is substantiated by use of different types of initial disturbances and by Blasius boundary-layer simulations. The present results point in the direction of universality of the observed transition mechanisms for localized disturbances in wall-bounded shear flows.

1. Introduction

The importance of three-dimensional components in the process of transition to turbulence has become widely recognized, and a growing amount of interest is being paid to the scenario of transition from strongly three-dimensional perturbations in the form of localized disturbances or simply oblique waves. The fact that the infinitesimal wave that first becomes unstable when the Reynolds number passes the critical value is a two-dimensional one lead to a focusing of interest, in the early studies of transition, on purely two-dimensional waves or disturbances with the dominating part of the energy in the two-dimensional wave component (see e.g. the review article of Reshotko 1976).

† Also at The Aeronautical Research Institute of Sweden (FFA), Bromma.

For infinitesimal amplitudes the disturbance development for a parallel mean flow is governed by the Orr–Sommerfeld (OS) equation supplemented by a non-homogeneous equation for the vorticity component in the wall-normal direction. For purely two-dimensional waves the forcing term is zero in the latter equation and the homogeneous part is associated with damped so-called Squire (SQ) modes. For oblique waves, and three-dimensional disturbances in general, a new element enters the problem in that a non-zero forcing term appears for the normal vorticity. This forcing is directly proportional to the spanwise derivative of the normal velocity and leads to qualitatively new possibilities for disturbance growth as compared to the case with two-dimensional waves. The importance of spanwise variation of the velocity components in the transition process was brought to particular attention by the boundary-layer experiments of Klebanoff, Tidstrom & Sargent (1962) who recognized that rapid growth of three-dimensional distortions of a primary two-dimensional finite-amplitude wave is largely responsible for the explosive breakdown to turbulence in this type of scenario.

Subsequent studies, theoretical and experimental, have shown that several different three-dimensional growth mechanisms exist within the concept of secondary instability of superimposed oblique waves on a finite-amplitude two-dimensional primary wave (for a review of the recent literature, see Herbert 1988 and Bayly, Orszag & Herbert 1988). The agreement is excellent between theoretical predictions based on Floquet theory and experimental observations of the early part of the evolution of the oblique waves both for the fundamental (or K-type) and the subharmonic types of instability. Both these instabilities develop into lambda vortices. In the fundamental type they occur aligned in the streamwise direction, whereas for the subharmonic case they occur in a staggered pattern. Detached shear layers in the streamwise velocity form above the lambda structures. The shear layers then intensify, become elongated and roll up, which in the experimental observations has been described in terms of low-velocity spikes.

Direct numerical simulations play an increasingly important role in investigations of these phenomena and for transition research in general (see e.g. the recent review of Kleiser & Zang 1991). The early stages of the fundamental type of secondary instability in the boundary layer was simulated by Murdock (1986). Spalart & Yang (1987) allowed the three-dimensional disturbances to develop from random noise superimposed on the primary wave in a box with large spanwise extent. Both fundamental and subharmonic secondary instability processes have now been studied through direct numerical simulations (see e.g. Fasel, Rist & Konzelmann 1990). The secondary instability processes exist in boundary layers as well as channel flow, and in the latter case, operate at Reynolds numbers, Re, down to roughly 1000 (based half-width and centreline velocity). This is also in the lower end of the regime where experiments have shown that regions of turbulence can be sustained and grow.

Transition in channel flow has been investigated through direct numerical simulations for over a decade (Orszag & Kells 1980; Orszag & Patera 1983). Secondary and tertiary instabilities in plane Poiseuille flow were studied via use of simulations by Zang & Krist (1989). They demonstrated that the growth of the oblique waves is strongly dependent on the coexistence of a mode with zero streamwise wavenumber ($\alpha = 0$), a fact that has also been noted in earlier investigations. In fact, they showed that an amplitude of the $\alpha = 0$ mode comparable to that of the oblique wave is a prerequisite for the onset of the growth in the fundamental secondary instability. This was further illustrated by reduced growth rates in simulations where the $\alpha = 0$ mode was artificially suppressed. This was particularly conspicuous in the situation at

strongly subcritical Reynolds numbers. We will later see the primary importance of $\alpha = 0$ components in the algebraic instability and subsequent breakdown of localized disturbances. The complete transition process in channel flow, starting with the fundamental secondary instability process, was treated by Gilbert (1988) (see also Gilbert & Kleiser 1990) in an accurate direct simulation at $Re = 5000$.

Although the secondary instability operates at subcritical Reynolds numbers the presumed initial state consisting of a finite-amplitude two-dimensional wave is highly unlikely to occur spontaneously in channel flow or in non-inflexional flows in general (Schubauer & Skramstad 1947). Significant three-dimensional developments are indeed likely to occur in natural transition before a two-dimensional equilibrium state is reached. Note also that exponential growth rates in non-inflexional flows are quite small even at large Reynolds numbers. The maximum growth rate in channel flow (attained at $Re \approx 48000$) corresponds to a tenfold increase in amplitude in about 150 channel widths (Bayley *et al.* 1988).

In studies using numerical simulations some investigators have tried to let the natural selection processes determine the preferred two- and three-dimensional instability mechanisms. Kim & Moser (1989) used an initial disturbance field in channel flow consisting of random numbers and found a preferred selection of longitudinal vortex modes. These essentially $\alpha = 0$ modes may be expected to appear in this process since they are only marginally damped (damping rate is $O(1/Re)$ at infinitesimal amplitudes for $\alpha = 0$). The Squire (1933) theorem has sometimes been misinterpreted to mean that two-dimensional waves are always the least stable ones and that most transition processes start with two-dimensional waves. One should keep in mind, however, that at subcritical Reynolds numbers the damping of the highly oblique waves may be smaller than for the least-damped two-dimensional wave. The highly oblique waves can also experience rapid algebraic growth. For a small-amplitude disturbance with spanwise but no streamwise variation Ellingsen & Palm (1975) showed that in the inviscid case the streamwise velocity component grows linearly, i.e. algebraically, with time.

In natural transition flow perturbations are likely to emanate from spatially localized effects such as surface irregularities. A natural approach to the study of such transition processes is therefore to investigate the development of different types of localized disturbances. In the present study we focus on subcritical disturbances which initially exhibit a strong degree of three-dimensionality.

Landahl (1980) analysed a localized disturbance and found that the disturbance energy in inviscid flows grows at least linearly in time if wavenumbers with a zero streamwise component are excited. In physical space this is manifested as an elongation of the disturbance in addition to the growth in amplitude. Hultgren & Gustavsson (1981) extended this analysis to show that the algebraic growth persists in the viscous case for the initial phase of the evolution, but that eventually viscous damping leads to decay. They also showed that the algebraic growth in boundary layers is associated with the continuous spectra of the Orr–Sommerfeld and Squire equations for large streamwise scales. In channel flow a viscous analysis of the evolution (Henningson 1991) shows that the growth can be regarded as an effect of a near resonance between slightly damped, highly oblique Orr–Sommerfeld and Squire modes. The initial growth rates in this transient type of evolution are usually orders of magnitude larger than typical viscous growth rates found in unstable shear flows (Gustavsson 1991; Henningson 1991).

To study the evolution of localized disturbances theoretically the initial value problem is the natural starting point. A Fourier–Laplace solution to the viscous linear

initial value problem in plane Couette flow was presented by Gustavsson & Hultgren (1980). When the Laplace integral is inverted the solution can be written as a sum of linear eigenmodes. If a continuous spectrum is present, such as for boundary-layer flows, it also appears naturally in the Laplace inversion (see Gustavsson 1979). For bounded flows, where the normal modes have been shown to form a complete set (DiPrima & Habetler 1969), one may directly assume that the solution can be written as a sum of the eigenmodes. This approach has been outlined by, among others Schensted (1961) and Eckhaus (1965) for two-dimensional flows and by Henningson & Schmid (1992) for the three-dimensional case.

The evolution of finite-amplitude disturbances can also be studied using the expansion technique. If the flow variables are expanded in eigenmodes of the linearized problem the nonlinearity will appear as quadratic interactions between the modes. Eckhaus (1965) derived the complete solution for two-dimensional plane Poiseuille flow in this manner and the solution for the three-dimensional case is discussed by Henningson & Schmid (1992).

The numerical simulations of localized vortical structures by Henningson, Johansson & Lundbladh (1990) indicated that the algebraic growth also plays an important role for finite-amplitude disturbances. It was found that energy was transferred to higher spanwise wavenumbers due to nonlinear interactions between the initially most energetic modes and waves exhibiting algebraic growth. The preferential excitation of components with higher spanwise wavenumbers appears to be quite general and is also indicated by the results of Breuer & Landahl (1990) in their boundary-layer investigation of finite-amplitude disturbances, as well as by Cohen, Breuer & Haritonidis (1991) in a study of the nonlinear breakdown of a wave packet. This nonlinear mechanism will be studied in detail in the present paper.

Disturbance growth and breakdown on a timescale much shorter than those typical for Tollmien–Schlichting (TS) waves has been called *bypass transition* (see Morkovin 1969), a term used to emphasize that these scenarios bypass the growth of two-dimensional waves and their subsequent secondary instability. Localized disturbances, such as those associated with surface roughness or other local conditions generating three-dimensionality, typically result in bypass transition by rapidly achieving finite amplitudes so that nonlinear effects can enter into play. Disturbances of large enough amplitude for nonlinear effects to dominate immediately may of course also cause bypass transition.

When a finite-amplitude localized disturbance breaks down, a turbulent spot is created, i.e. a localized region of turbulence in an otherwise laminar flow. Turbulent spots have been studied in a number of flow situations (for references see e.g. Riley & Gad-el-Hak 1985), among them the boundary-layer and plane channel flows. Direct numerical simulations of turbulent spots have been carried out in plane Poiseuille and boundary-layer flows (Henningson, Spalart & Kim 1987 and Bullister & Orszag 1987) and recently in plane Couette flow (Lundbladh & Johansson 1991). The details of the underlying mechanisms for the formation of a turbulent spot are still unclear and one aim of the present investigation is to map out a transition scenario that produces a turbulent spot through use of high-resolution direct simulations.

The present study is aimed at investigating possible mechanisms for bypass transition from localized disturbances in wall-bounded shear flows with non-inflexional mean velocity profiles. Particular attention is paid to the plane Poiseuille flow case. The development phases from linear through weakly nonlinear to the subsequent breakdown are analysed and treated through use of direct numerical simulation techniques as well as by eigenfunction and amplitude expansions. The generality of the

observed processes is discussed, and comparisons with simulations for other types of localized disturbances and boundary-layer flow are also made. These point in the direction of universality of the breakdown processes.

2. Base flow and initial disturbance

The major effort in the present investigation will be concentrated on localized disturbances in plane Poiseuille flow. In order to show that the mechanisms uncovered are not solely related to that flow we will also consider the Blasius boundary layer. In Poiseuille flow all quantities are normalized by the centreline velocity (U_{CL}) and the channel half-height (h), whereas the corresponding quantities in the boundary layer are taken to be the free-stream velocity (U_∞) and the displacement thickness (δ_*). When similar features of the two flows are compared we have chosen to rescale the Poiseuille flow results in terms of an equivalent displacement thickness, calculated based on the Poiseuille profile in the lower part of the channel. Since that thickness is a third of the channel half-height the non-dimensionalized time and space variables for the channel results are multiplied by three when a comparison with the boundary layer is made.

In Poiseuille flow we chose a Reynolds number (R) of 3000, since our interest is in exploring transition mechanisms that are different from exponential growth of TS waves. Recall that the critical Reynolds number for the onset of such growth is 5772 (Orszag 1971). We focus on structures initially consisting of two pairs of counter-rotating vortices of the form

$$\psi = \epsilon f(y)\,(x'/l_x)\,z' \exp\left[-(x'/l_x)^2-(z'/l_z)^2\right], \tag{1a}$$

$$(u, v, w) = (-\psi_y \sin\theta, \psi_{z'}, -\psi_y \cos\theta), \tag{1b}$$

$$(x', z') = (x\cos\theta - z\sin\theta, x\sin\theta + z\cos\theta). \tag{1c}$$

Here (x, y, z) and (u, v, w) are the streamwise, normal, and spanwise coordinates and disturbance velocities, respectively, l_x and l_z the streamwise and spanwise lengthscales of the disturbance and ϵ its amplitude. The normal dependence was chosen as

$$f(y) = (1+y)^p\,(1-y)^q, \tag{2}$$

with $p = q = 2$.

The horizontal scales of the disturbance in plane Poiseuille flow were chosen as $l_x = l_z = 2$ for the results presented here. Other choices were tested and the results were found to be rather insensitive to the specific values of l_x and l_z. Three different amplitudes were used in the channel flow simulations. For small, moderate and large amplitudes ϵ was chosen as 0.0001, 0.0699 and 0.1398, corresponding to a maximum initial normal velocity amplitude of 0.000043, 0.03 and 0.06.

The angle θ of the disturbance was used as a parameter enabling the initial energy to be distributed in different regions of wavenumber space. Note that when the disturbance is rotated in physical space around the y-axis, the energy spectrum is rotated by the same angle around the origin in wavenumber space. The initial disturbance can be seen in figure 1.

To investigate the sensitivity of the growth mechanisms to the specifics of the initial disturbance a qualitatively different initial disturbance was studied. An initial velocity field lacking normal vorticity was achieved by an axisymmetric disturbance.

$$\psi = \tfrac{1}{2}\epsilon f(y)\, r^2\, \mathrm{e}^{-(r/l)^2}, \tag{3a}$$

$$(u, v, w) = \left(-\frac{x}{r^2}\psi_y, \frac{1}{r}\psi_r, -\frac{z}{r^2}\psi_y\right)\mathrm{e}^{(r/l)^2}, \tag{3b}$$

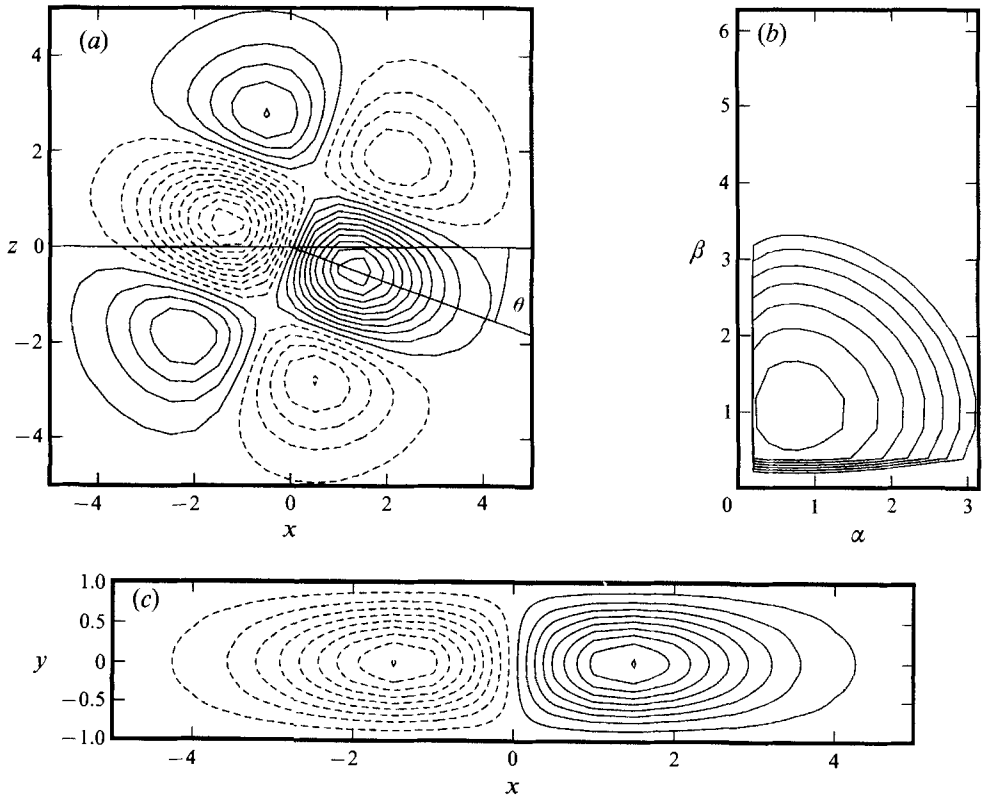

FIGURE 1. Initial normal velocity with $\epsilon = 0.0001$. (*a*) $y = -0.56$, $\theta = 20°$, contour spacing 2.0×10^{-6}. (*b*) Power spectrum integrated in the normal direction for $\theta = 0$, contour spacing 1 decade. (*c*) $z = 0$, $\theta = 0$, contour spacing 5.0×10^{-6}.

where $f(y)$ is taken as in (2) with $p = 2$ and $q = 5$, $r^2 = x^2 + y^2$ and $l = 2$. Note that this disturbance has its highest amplitudes at the bottom of the channel and introduces both symmetries in the normal direction. This disturbance was run with two different amplitudes, $\epsilon = 0.0138$ and 0.0276. They were matched such that the energy contained in them was the same as in the moderate- and large-amplitude cases above. This gave a maximum of the initial normal velocity which was slightly lower than for the corresponding counter-rotating vortex disturbance.

In boundary-layer flow we use the disturbance (1) with

$$f(y) = (y/l_y)^3 \exp\left[-(y/l_y)^2\right] \tag{4}$$

and the lengthscales $l_x = 5$, $l_y = 1.2$, $l_z = 6$, i.e. the same values as in Breuer & Haritonidis (1990) and Breuer & Landahl (1990). The Reynolds number chosen, 950, was also the same as in their investigation. For small, moderate and large amplitudes ϵ was chosen as 0.001, 0.2 and 0.7, corresponding to maximum initial normal velocity amplitude of approximately 0.00003, 0.006 and 0.02.

The type of disturbance described by (1) has been used earlier in studies of transition starting with localized disturbances. Henningson (1988) used it in an inviscid model for the channel flow problem and Breuer & Landahl (1990) studied this type of disturbance numerically in an investigation of finite-amplitude effects in the boundary layer. It has also been found to correspond to experimentally induced perturbations caused by the motion of a membrane at the wall (Breuer & Haritonidis 1990). In the experiment the

membrane moved up and down once, after which it was kept flush with the wall surface. In these earlier investigations the vortices were aligned with the mean flow direction. The new effects caused by varying the angle θ have not previously been studied.

3. Numerical simulation method

In the following sections numerical simulation results will be presented, where a spectral method is used to solve the Navier–Stokes equations, with Fourier representation in the streamwise and spanwise directions, and Chebyshev polynomials in the wall-normal direction. The nonlinear terms are treated pseudo-spectrally using FFTs, in a manner similar to that of Kim, Moin & Moser (1987). Although, here, instead of the variables themselves, their second-derivatives are expanded in Chebyshev series (Greengard 1988). This results in better numerical accuracy since the need for the evaluation of ill-conditioned Chebyshev derivatives is virtually eliminated. The time advancement used was a third-order Runge–Kutta method for the nonlinear terms and a second-order Crank–Nicholson method for the linear terms, with a time step dynamically kept at 90% of the theoretical CFL limit. Aliasing errors from the evaluation of the nonlinear terms were removed by the $\frac{3}{2}$-rule when the horizontal FFTs were calculated. The complete numerical method for the channel flow geometry is described in Lundbladh, Henningson & Johansson (1992). The code has previously been used in the studies by Henningson *et al.* (1990) and Lundbladh & Johansson (1991).

The boundary-layer computations were carried out with a code based on the same numerical methods as for Poiseuille flow. The domain was truncated in the wall normal direction well out in the constant-velocity region. At that outer boundary a free-stream boundary condition derived from an explicit solution of the potential flow equations in the free stream was used (see Malik, Zang & Hussaini 1985). The boundary layer was represented as a temporally growing parallel flow by application of a weak volume force which retained a Blasius velocity profile for the undisturbed flow.

Two types of numerical truncation errors are introduced in these computations, one from the limited spatial resolution and one from the periodic boundary conditions enforced on a finite computational box. For small- and moderate-amplitude disturbances both the box size and the resolution were systematically varied to show that all results presented below are accurate, even in details, to the precision of the graphics used. In table 1 the parameters used for the main simulation cases are reproduced. For initial disturbances with spanwise symmetry the conservation of this symmetry by the Navier–Stokes equations was made use of in order to reduce the number of computational modes.

In Poiseuille flow the large-amplitude disturbance was followed up to and through the breakdown stage, which required a substantially higher resolution than the moderate-amplitude simulations. In table 1 two simulations of this disturbance are listed. When the second run, with a higher spatial resolution but a smaller box, was compared to the first one it showed no significant differences in the breakdown features, demonstrating that both types of truncation errors were negligible. A number of simulations with various lower resolutions showed that only the two higher resolutions could be considered converged for all stages of the transition process. At lower resolutions spurious numerical instabilities appear with a character resembling that of a physical secondary instability.

As a measure of the difficulty involved in resolving all scales through the breakdown

Flow	Disturbance	Amplitude	Computational domain	Number of modes
Poiseuille	vortex pairs	small	$48\times2\times24$	$96\times65\times96$
Poiseuille	vortex pairs	moderate	$48\times2\times24$	$96\times65\times192$
Poiseuille	vortex pairs	large	$53\times2\times27$	$512\times97\times512$
Poiseuille	vortex pairs	large	$33\times2\times13$	$400\times121\times320$
Poiseuille	axisymmetric	moderate	$48\times2\times24$	$96\times65\times192$
Poiseuille	axisymmetric	large	$33\times2\times13$	$320\times97\times256$
boundary layer	vortex pairs	small	$100\times8\times50$	$80\times65\times80$
boundary layer	vortex pairs	moderate	$100\times8\times50$	$80\times65\times80$
boundary layer	vortex pairs	large	$80\times8\times32$	$256\times109\times192$

TABLE 1. Parameters for the main simulation cases. For initial disturbances with spanwise symmetry the number of computational modes in the spanwise direction was half of that indicated. Note that each item may represent a number of individual simulations. For dealiasing purposes the number of gridpoints was 3/2 times the number of modes in each of the horizontal directions.

stages, we mention that the total amount of computer time spent in this study was about 600 CRAY CPU hours. The largest individual run took 150 CPU hours and 100 MWords of memory. It was run in parallel on four CRAY-2 processors.

In the later stages when a small turbulent spot is formed a wall scaling can be used to assess the effective resolution. With an estimated friction velocity from the turbulent part, Δx^+ and Δz^+ are roughly 11 and 5 for the best resolved computation (corresponding to 7 and 3.5 on the dealiazed grid). This slightly better than in the Kim *et al.* (1987) turbulent channel flow simulation.

4. Theoretical considerations

In order to be able to elucidate linear and nonlinear mechanisms in the growth, spreading and breakdown of localized disturbances we briefly discuss the theoretical background. The vector-mode notation of Henningson & Schmid (1992) for the normal velocity–normal vorticity formulation of the disturbance equations is particularly convenient for the purposes of the present investigation and will be adopted here. Other approaches have been used by several previous investigators (references additional to those given below can be found in the article by Henningson & Schmid).

4.1. *Governing equations*

We start with the complete disturbance equations in normal velocity–normal vorticity form. We will assume that the dependent variables can be expanded in Fourier series in the horizontal directions. Although this assumes periodicity, a localized disturbance can still be considered as long as the period is large enough. This formulation also conforms to the representation of the disturbance used in the numerical simulation program. For the streamwise and spanwise wavenumber combination (α_m, β_n) the complete disturbance equations can be written

$$\frac{\mathrm{d}}{\mathrm{d}t}\mathbf{M}\hat{\boldsymbol{q}}_{mn} + \mathbf{L}\hat{\boldsymbol{q}}_{mn} = \sum_{\substack{k+i=m \\ l+j=n}} N(\hat{\boldsymbol{q}}_{kl}, \hat{\boldsymbol{q}}_{ij}), \tag{5}$$

where

$$\hat{\boldsymbol{q}}_{mn} = \begin{pmatrix} \hat{v}_{mn} \\ \hat{\eta}_{mn} \end{pmatrix}, \quad \mathbf{M} = \begin{pmatrix} -\mathrm{D}^2 + k_{mn}^2 & 0 \\ 0 & 1 \end{pmatrix}, \quad \mathbf{L} = \begin{pmatrix} \mathrm{L_{OS}} & 0 \\ \mathrm{i}\beta_n U' & \mathrm{L_{SQ}} \end{pmatrix},$$

where $\hat{\eta}_{mn}$ is a Fourier coefficient of the normal vorticity. L_{OS} and L_{SQ} are related to the OS and SQ operators, respectively, and are defined

$$L_{OS} = -i\alpha_m U(D^2-k_{mn}^2)+i\alpha_m U''+(D^2-k_{mn}^2)^2/R, \tag{6a}$$

$$L_{SQ} = i\alpha_m U-(D^2-k_{mn}^2)/R. \tag{6b}$$

N is the nonlinear right hand side, $k_{mn}^2 = \alpha_m^2+\beta_n^2$ and $U(y)$ is the mean flow in the streamwise direction. The double convolution sum represents the nonlinear triad interactions. For an explicit form of the nonlinear operator in (5) see Henningson & Schmid (1992).†

From these equations, together with the initial and boundary conditions

$$\hat{v} = \hat{v}_0(\alpha, y, \beta), \quad \hat{\eta} = \hat{\eta}_0(\alpha, y, \beta), \quad t = 0, \tag{7}$$

and

$$\hat{v} = D\hat{v} = \hat{\eta} = 0, \quad y = \pm 1 \tag{8}$$

the complete disturbance development may be calculated. The horizontal velocities can then be obtained from

$$\hat{u} = \frac{i}{k^2}(\alpha D\hat{v}-\beta\hat{\eta}), \quad \hat{w} = \frac{i}{k^2}(\beta D\hat{v}+\alpha\hat{\eta}), \tag{9a, b}$$

which is derived using the continuity equation and the definition of the normal vorticity.

For a localized disturbance the rate of growth or decay of the total disturbance energy is an important measure of the stability of the flow. It is here illustrative to write the kinetic energy for a specific Fourier component, E_{mn}, in the form

$$E_{mn} = \frac{1}{2k_{mn}^2}\int_{-1}^{1} \hat{\boldsymbol{q}}_{mn}^{H}\mathbf{M}\hat{\boldsymbol{q}}_{mn}\,dy = \frac{1}{2k_{mn}^2}\int_{-1}^{1}(|D\hat{v}_{mn}|^2+k_{mn}^2|\hat{v}_{mn}|^2+|\hat{\eta}_{mn}|^2)\,dy. \tag{10}$$

where superscript H denotes complex conjugate transpose. This identity is readily derived by use of Parseval's relation and (9*a*) and (9*b*) above (see also Gustavsson 1986). The total disturbance energy is obtained if the above expression is summed over all excited wavenumbers.

In the assessment of the role of linear and nonlinear processes in the finite-amplitude development of a disturbance it is useful to consider the energy transfer into a particular Fourier mode. Using (5), (8) and (10) that can be written

$$\frac{d}{dt}E_{mn} = \frac{1}{k_{mn}^2}\mathrm{Re}\left(-\int_{-1}^{1}\hat{\boldsymbol{q}}_{mn}^{H}\mathbf{L}\hat{\boldsymbol{q}}_{mn}\,dy+\sum_{\substack{k+i=m\\ l+j=n}}\int_{-1}^{1}\hat{\boldsymbol{q}}_{mn}^{H}N(\hat{\boldsymbol{q}}_{kl},\hat{\boldsymbol{q}}_{ij})\,dy\right), \tag{11}$$

where Re signifies the real part of the subsequent complex expression. The first integral represents the rate of energy transfer due to the linear term and the second that due to the nonlinear wave triad interactions. When the total disturbance energy is calculated by summing (11) over all wavenumbers it is interesting to note that the nonlinear terms drop out. This follows from the Reynolds–Orr equation (see Drazin & Reid 1981, p.

† Note that for wavenumber zero ($\alpha = \beta = 0$) both the normal velocity and normal vorticity are zero, and that $\hat{\boldsymbol{q}}_{00}$ instead contains the streamwise and spanwise velocities. The governing operators for this case also require changes.

425), that governs the rate of change of the total disturbance energy, and can easily be understood from the fact that the nonlinear terms in the Navier–Stokes equations and corresponding terms in the energy equation can be written as a divergence. In the derivation of the Reynolds–Orr equation the base flow is taken as an exact solution to the Navier–Stokes equations. In the situation studied here we are left with

$$\frac{dE}{dt} = \frac{d}{dt}\sum_{mn} E_{mn} = \sum_{mn} \frac{1}{k_{mn}^2} \mathrm{Re}\left\{ -\int_{-1}^{1} \hat{\boldsymbol{q}}_{mn}^{\mathrm{H}} \mathbf{L} \hat{\boldsymbol{q}}_{mn} \, dy \right\}. \tag{12}$$

This shows that the relative change of the total energy is independent of the disturbance amplitude, i.e. at every instant the quantity $(1/E)\,(dE/dt)$ is unaffected by a rescaling of the amplitude. Hence, if all infinitesimal disturbances exhibit a monotonic decay of the total energy this will also be the case for finite amplitudes. Conversely, if any finite-amplitude disturbance exhibits total energy growth there must exist an instantaneously growing infinitesimal disturbance. Actually, the latter can readily be constructed by rescaling the finite-amplitude disturbance.

Despite the necessity of linear mechanisms for the existence of total energy growth and transition, nonlinear interactions affect the evolution of the disturbance and may therefore indirectly contribute to the energy growth. An important aspect of the nonlinear interactions is to redistribute the energy in wavenumber space to regions of large growth rate.

4.2. *Eigenfunction expansions and transient growth*

For small-amplitude disturbances the nonlinear terms of (5) can be neglected and the solution to the equation can be expressed as an expansion in the eigenmodes of the linear part of system. Once exponential time dependence has been assumed, the linear system can be written (if we drop the subscripts mn)

$$\begin{pmatrix} \mathrm{L_{OS}} & 0 \\ \mathrm{i}\beta U' & \mathrm{L_{SQ}} \end{pmatrix} \begin{pmatrix} \tilde{v} \\ \tilde{\eta} \end{pmatrix} - \mathrm{i}\omega \begin{pmatrix} -\mathrm{D}^2 + k^2 & 0 \\ 0 & 1 \end{pmatrix} \begin{pmatrix} \tilde{v} \\ \tilde{\eta} \end{pmatrix} = 0. \tag{13}$$

This equation has the same boundary conditions as (5). The eigenmodes of this system consist of both the OS and SQ modes. The part associated with the OS eigenvalues consists of a normal velocity component ($\tilde{v}$) which is a solution to the first component of (13) and a forced particular solution for the normal vorticity ($\tilde{\eta}^{\mathrm{p}}$). The forcing results from the off-diagonal term $\mathrm{i}\beta U'$. The part associated with the SQ eigenvalues consists solely of a homogeneous solution ($\tilde{\eta}$) of the second component of (13). The eigenfunction expansion may, hence, be written

$$\hat{\boldsymbol{q}} = \sum_{l=1}^{L} K_l \begin{pmatrix} \tilde{v}_l \\ \tilde{\eta}_l^{\mathrm{p}} \end{pmatrix} \mathrm{e}^{-\mathrm{i}\omega_l t} + \sum_{j=1}^{J} B_j \begin{pmatrix} 0 \\ \tilde{\eta}_j \end{pmatrix} \mathrm{e}^{-\mathrm{i}\sigma_j t}. \tag{14}$$

Here ω_l and σ_j are OS and SQ eigenvalues, respectively. The expansion coefficients are determined from the initial conditions using the eigenfunctions of the system adjoint to (13) and the appropriate bi-orthogonality conditions. The expansion coefficients are (see Henningson & Schmid 1992)

$$K_l = \int_{-1}^{1} \tilde{v}_l^{+*} (-\mathrm{D}^2 + k^2)\, \hat{v}_0 \, dy \tag{15a}$$

$$B_j = \int_{-1}^{1} [\tilde{v}_j^{\mathrm{p}+*} (-\mathrm{D}^2 + k^2)\, \hat{v}_0 + \tilde{\eta}_j^{+*}\, \hat{\eta}_0] \, dy. \tag{15b}$$

Here $\tilde{v}^+$ is a solution to the adjoint OS equation, $\tilde{\eta}^+$ is a solution to the adjoint SQ equation and $\tilde{v}^{p+}$ is the associated forced adjoint normal velocity.

The potential for algebraic or transient growth of the solution can be seen directly from (14). Suppose that we expand an initial condition with zero normal vorticity. This will excite a number of OS modes, in order to represent the normal velocity. Each OS mode has an associated particular normal vorticity ($\tilde{\eta}_l^p$), which now needs to be cancelled out by an appropriate combination of SQ modes. Thus, both OS and SQ modes are excited by an initial condition of zero normal vorticity. This has important implications for the disturbance development. As the perturbation evolves downstream each part propagates with the characteristics given by its eigenvalue. Since the phase speeds and decay rates are different the modes will propagate apart and the cancellation that occurred initially will not persist. Thus the disturbance will experience transient growth in the normal vorticity component. It should be noted that the particular normal vorticity in an OS mode is typically much larger than the normal velocity, thus giving rise to the cancellation effects even if the disturbance has a moderate initial normal vorticity. Both the particular normal vorticity and the resulting transient growth is largest for Fourier components with small streamwise wavenumbers.

The cancellation effects described above are only possible because of the non-orthogonality of the eigenmodes and are mathematically a result of the non-normality of the operators governing the above systems (an operator is normal if it commutes with its adjoint). Both orthogonality and adjoint are defined in the standard manner using the inner product associated with the energy norm (10). Solutions to problems governed by non-normal operators may only show the behaviour predicted by the associated eigenvalues as $t \to \infty$. Initially they are not necessarily mode-like and have the possibility of large transient growth although all eigenvalues predict decay. This behaviour has been seen in a number of different applications, including the analysis of the stability of numerical discretization schemes, the analysis of iterative methods in linear algebra and in the area of hydrodynamic stability. Some recent work is discussed in Reddy (1991) and Trefethen (1991). Hydrodynamic stability results can also be found in Farrell (1988), Butler & Farrell (1992) and Reddy, Schmid & Henningson (1993). Another related work is that of Gustavsson (1991), who uses somewhat different techniques.

The transient growth can also be described as forcing of the normal vorticity by the normal velocity, represented by the off-diagonal term $i\beta U'$ in the first matrix operator of (13). This term represents tilting of the mean spanwise vorticity such that normal perturbation vorticity is created.

The transient growth is largest for small streamwise wavenumbers and persist also in the inviscid case. To see this we will rewrite the normal vorticity part of the eigenfunction expansion. We expand the particular normal vorticity and the particular adjoint normal velocity in modes of their respective homogeneous operators. If these expansions are introduced into the second component of (14) and into (15*b*) we find

$$\hat{\eta} = \sum_{j=1}^{J} \int_{-1}^{1} \tilde{\eta}_j^{+*} \hat{\eta}_0 \, \mathrm{d}y \, \tilde{\eta}_j \mathrm{e}^{-\mathrm{i}\sigma_j t} - \sum_{j=1}^{J} \left[\sum_{l=1}^{L} \frac{\beta K_l}{\sigma_j - \omega_l} \int_{-1}^{1} U' \tilde{v}_l \, \tilde{\eta}_j^{+*} \, \mathrm{d}y \, (\mathrm{e}^{-\mathrm{i}\omega_l t} - \mathrm{e}^{-\mathrm{i}\sigma_j t}) \right] \tilde{\eta}_j. \quad (16)$$

In the limit of small αR the dependence of the OS and SQ eigenvalues on the Reynolds number can be found explicitly. If we use the expansion from Drazin & Reid (1981, p. 159) we can write the eigenvalues as

$$\omega_l = -\mathrm{i}\mu_l/R + O(\alpha), \quad \sigma_j = -\mathrm{i}\nu_j/R + O(\alpha) \quad (17a, b)$$

where μ_l and ν_j are real, positive and independent of Reynolds number. If these expressions are used in (16) and the result is Taylor expanded for small t/R we have

$$\hat{\eta} = \sum_{j=1}^{J} \int_{-1}^{1} \tilde{\eta}_j^{+*} \hat{\eta}_0 \, \mathrm{d}y \, \tilde{\eta}_j \, \mathrm{e}^{-\mathrm{i}\sigma_j t} - \mathrm{i}\beta t \sum_{j=1}^{J} \left\{ \sum_{l=1}^{L} K_l \int_{-1}^{1} U' \tilde{v}_l \tilde{\eta}_j^{+*} \, \mathrm{d}y \left[1 - (\nu_j + \mu_l) \frac{t}{R} + O\left(\alpha R \frac{t}{R}, \frac{t^2}{R^2} \right) \right] \right\} \tilde{\eta}_j. \quad (18)$$

By a summation of the expansions the leading-order term can be written

$$\hat{\eta} = (\hat{\eta}_0 - \mathrm{i}\beta U' \hat{v}_0 \, t)[1 + O(\alpha t, t/R)], \quad (19)$$

which clearly shows that there may be substantial algebraic growth for $\beta \neq 0$ if $\alpha t \ll 1$ and $t/R \ll 1$.

For viscous flow with Reynolds numbers in the range considered presently the condition $t/R \ll 1$ is fulfilled for moderate times. The additional condition $\alpha t \ll 1$, however, shows that there has to be energy in low streamwise wavenumbers for substantial growth to occur. If the latter condition is the limiting factor we should expect to see energy growth for times such that $t \ll 1/\alpha^*$, if a significant amount of energy is contained in streamwise wavenumbers on the order of α^* or less.

For the idealized case where we consider $\alpha = 0$ equation (18) clearly shows that the maximum amplitude is of order R and occurs for times of order R. This behaviour was found by Gustavsson (1991) in a detailed investigation of growth for the $\alpha = 0$ case. This behaviour is, however, of somewhat limited importance for the localized disturbances considered here since only a small fraction of the energy is contained in wavenumbers satisfying $\alpha R \ll 1$. In the numerical investigations it was also found that the maximum amplitude typically is a small fraction of R.

The result in (19) may also be interpreted as the inviscid limit if we let $R \to \infty$. This limit shows that there is algebraic growth for all times for inviscid disturbances which are independent of the streamwise direction. This inviscid *algebraic instability* was first found by Ellingsen & Palm (1975) who derived an expression equivalent to (19). Thus (18) shows that the growth experienced by zero streamwise wavenumber components is essentially caused by an inviscid mechanism whereas the subsequent decay is a result of viscous effects. Landahl (1975) termed the mechanism of growth due to the $U'v$ term *lift-up* since it can be directly related to the velocity defect created when a fluid particle is lifted up in the direction normal to the wall while keeping its horizontal momentum constant. Landahl (1980) also showed that although the inviscid instability only operates for zero streamwise wavenumbers it still causes unbounded energy growth for localized disturbances if wavenumbers with $\alpha = 0$ are excited.

5. Linear evolution

5.1. *Direct numerical simulation results*

In order to ensure negligible nonlinear effects over the time period studied the amplitude parameter of the initial disturbance was chosen as $\epsilon = 0.0001$ in the numerical simulation. The linear evolution of the normal velocity field for $\theta = 0$ is seen in figure 2(*a*) to be associated with the dispersion of a wave packet. Owing to the dispersive effects and the damping of the normal modes the amplitudes decrease by about one order of magnitude between $t = 10$ and 40. The wave packet structure can

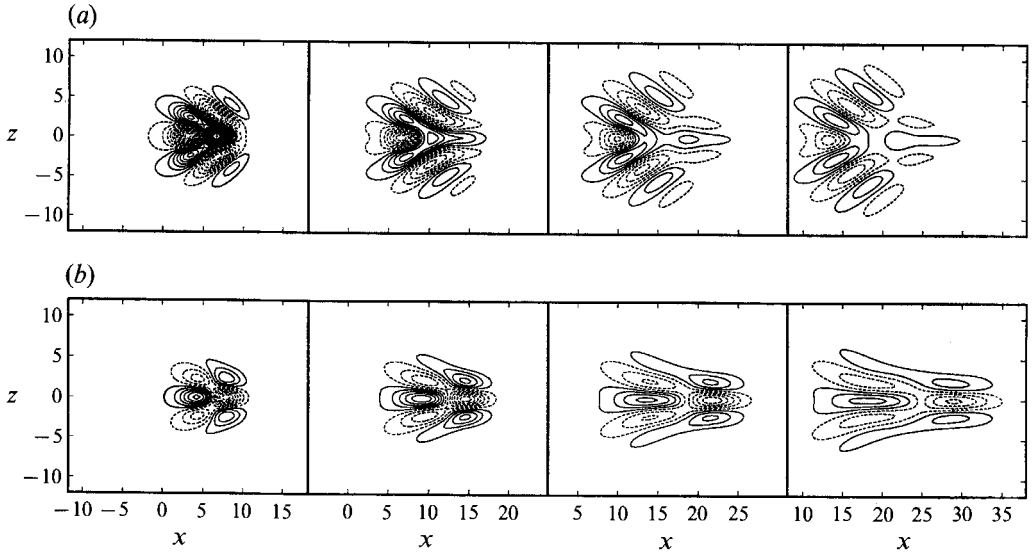

FIGURE 2. Small-amplitude disturbance at $y = -0.56$, $\theta = 0$, $t = 10, 20, 30, 40$: (*a*) normal velocity, (*b*) streamwise velocity. Contour spacing: v, 1.0×10^{-6}; u, 2.0×10^{-5}.

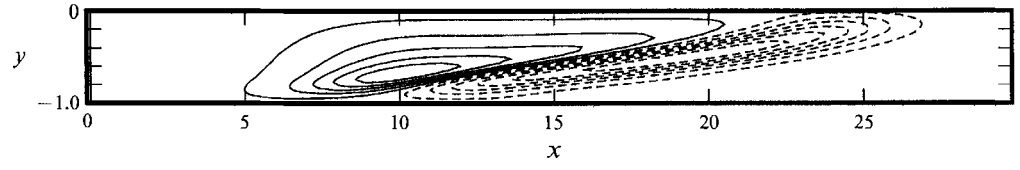

FIGURE 3. Streamwise velocity of a small-amplitude disturbance at $z = 0$, $t = 25$, $\theta = 0$. Contour spacing 2.0×10^{-5}.

also be observed in the associated streamwise velocity (figure 2*b*), although the main flow feature is now a strong streamwise shear layer that has developed around the symmetry plane (figure 3). Note that the streamwise velocity has an amplitude which is about one order of magnitude larger than the normal velocity, although no streamwise velocity was present initially. This growth is due to the three-dimensional linear mechanism discussed in §4.2 and was also found in the boundary-layer experiments by Breuer & Haritonidis (1990) who investigated the development of the shear layer in detail. The shear layer in figure 3 can be compared with figure 4 of Breuer & Haritonidis. We compare the flow features at a time which is equivalent if scaled with the maximum streamwise velocity and the displacement thickness. This scaling is motivated by the inviscid nature of the growth mechanism. The comparison shows that all the qualitative features are the same in the two cases.

If the initial disturbance is rotated about the y-axis (see figure 1) new features can be seen in the development (figure 4). The streamwise amplitude of the disturbance grows more rapidly, and at $t = 40$ the disturbance is considerably more streaky. In contrast to the $\theta = 0$ simulation the spanwise shear now dominates.The increase in amplitude growth with θ can be seen in figure 5(*a*). The contrast between the rapid algebraic growth for $\theta = 45°$ and the decay for $\theta = 0$ is conspicuous. The results confirm that the maximum growth occurs when the energy of the initial disturbance is centred around the algebraically growing modes along the spanwise wavenumber axis.

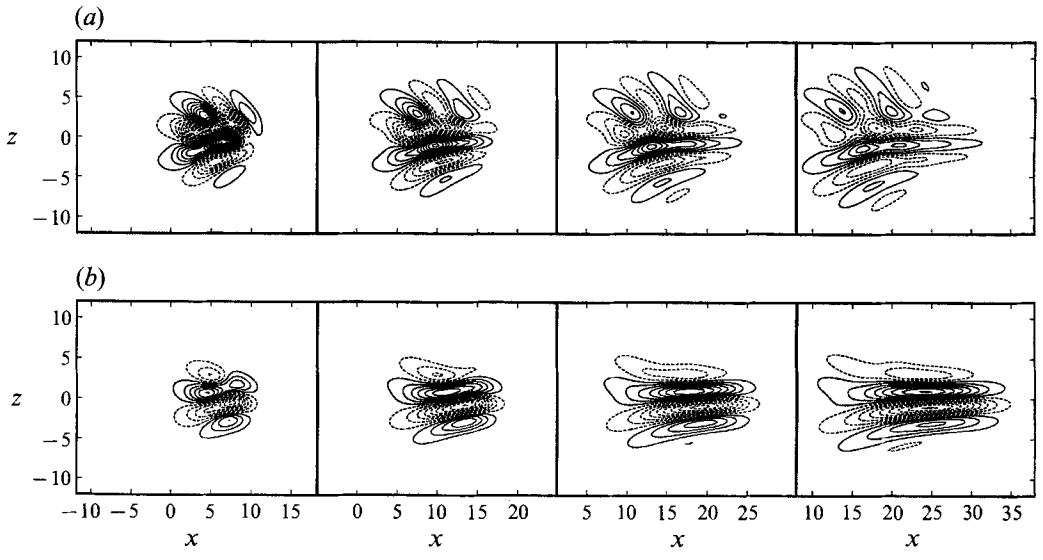

FIGURE 4. Small-amplitude disturbance at $y = -0.56$, $\theta = 20$, $t = 10, 20, 30, 40$: (*a*) normal velocity, (*b*) streamwise velocity. Contour spacing: v, 1.0×10^{-6}; u, 2.0×10^{-5}.

Recall that turning the disturbance 45° in physical space also turns the spectrum the same amount in wavenumber space, thus centring a major part of the energy around $\alpha = 0$.

One should remember that although the energy grows for $\theta = 45°$ over the time period studied here, eventually the exponential damping will dominate. The maximum in energy is, however, shifted to larger times, and its magnitude becomes larger with increasing initial disturbance energy in low streamwise wavenumbers. This effect increases with Reynolds number so that inviscid disturbances with energy along the spanwise wavenumber axis consequently grow for all times (see (19)).

The energy growth is associated with the generation of normal vorticity through forcing by the normal velocity. This part of the disturbance energy (i.e. $(1/k^2)\hat{\eta}\hat{\eta}^*$) is initially the same for all angles θ, but grows more rapidly with increasing angle. It also constitutes practically all of the energy after relatively short times (figure 5*b*). For instance, at $t = 15$ for $\theta = 0$, about 76% of the total energy resides in the u-component, whereas, in terms of the alternative energy decomposition, about 96% can be ascribed to the normal-vorticity-related part. The distribution of the energy among the components of the alternative decomposition is essentially the same for the cases with $\theta \neq 0$.

5.2. *Eigenfunction expansion results*

The results from the simulations can be reproduced using the eigenfunction expansion. We use the expansion (14) where the coefficients are calculated using expressions (15*a*) and (15*b*). Note that we have to include a number of streamwise and spanwise Fourier components to capture the streamwise and spanwise variation of the localized disturbance. For each such wavenumber a number of normal modes have to be used.

Figure 6 shows the time evolution of the r.m.s. values of the normal velocity and the normal vorticity for the localized disturbance. One, four, ten, fifteen and twenty of the least stable modes are used in the eigenfunction approximations. Four modes capture the behaviour of the normal velocity after $t = 20$ whereas one mode is sufficient after $t = 30$. The cases with a larger number of modes fall on top of the data obtained from

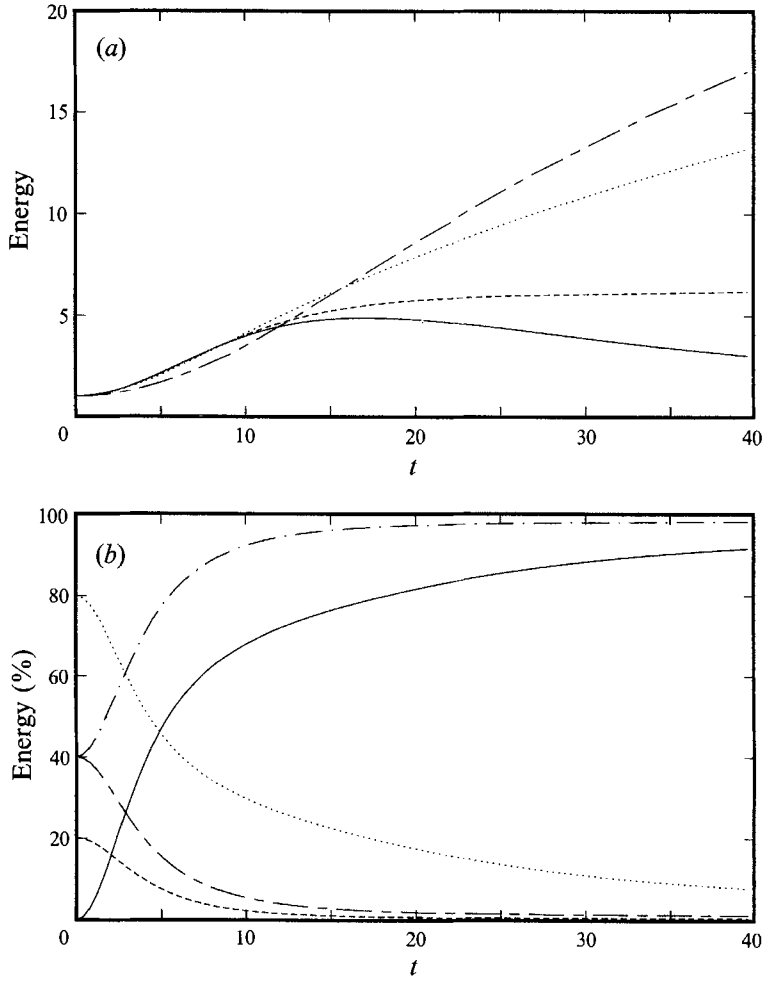

FIGURE 5. Energy for the small-amplitude disturbances. (*a*) ——, $\theta = 0$; – – –, $\theta = 10°$; · · · · · ·, $\theta = 20°$; – – – –, $\theta = 45°$; normalized by initial energy. (*b*) Percentage contribution for $\theta = 0$ from: ——, u; – – –, v; · · · · · ·, w; – – – –, Dv; – · – · –, η.

the numerical simulation. The convergence of the expansion for the normal vorticity is not as regular. We have to increase the number of modes to a total of 40 (20 OS and 20 SQ modes) to be able to capture the initial transient growth phase.

There is a large initial cancellation between non-orthogonal modes causing the transient growth. After the peak there is mode-like behaviour as the least-stable eigenvalues govern the decay. The fact that the expansions with insufficient number of modes overshoots initially for the normal vorticity component is again a result of the non-orthogonality of the modes. If the modes were orthogonal all partial sums would have a smaller energy than the exact solution.

We will consider the mode excitation in detail for $\alpha = \beta = 1.0472$, which is a wavenumber located approximately at the peak of the initial normal vorticity in wavenumber space. Figure 7 shows the OS and SQ eigenvalues for that wavenumber combination and the initial excitation of these modes is given in table 2. The expansion coefficients in the table are normalized such that a mode with coefficient unity would have unit energy if the mode contained all of the initial energy of the disturbance. The

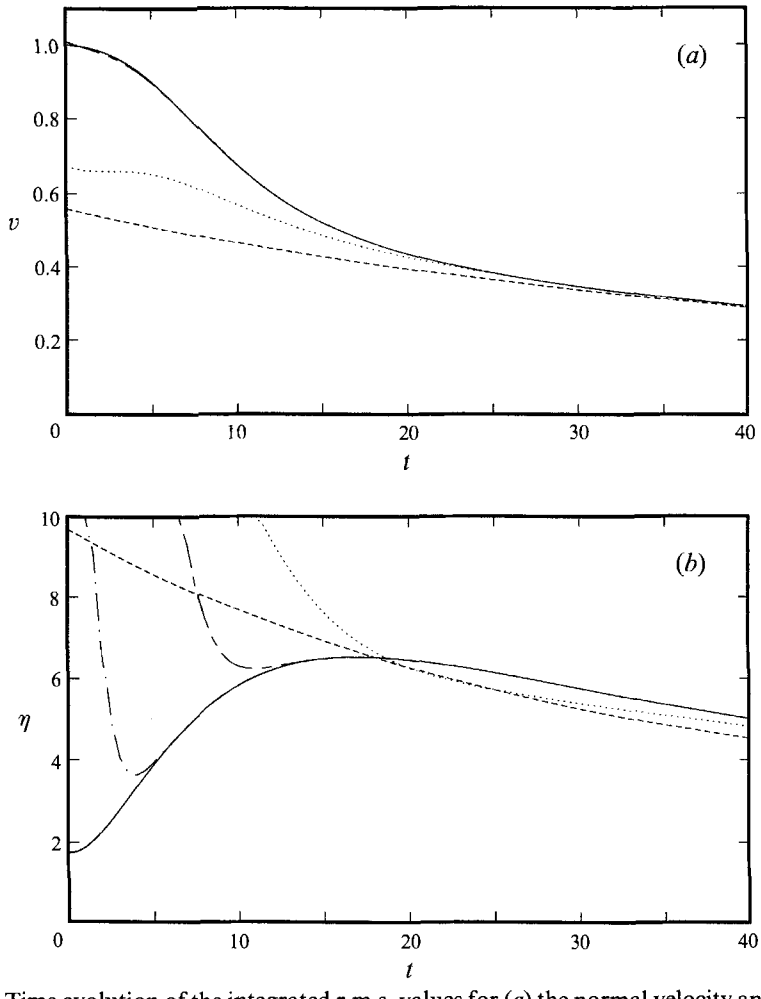

FIGURE 6. Time evolution of the integrated r.m.s. values for (*a*) the normal velocity and (*b*) the normal vorticity. Solid curves represents the numerical simulations, while the dashed, dotted, chain-dashed and chain-dotted curves represent the eigenfunction expansions using $L = J = 1$, 4, 10 and 15 respectively. The curves for $L = J = 20$ are also included but cannot be distinguished from the numerical simulation results.

modes are labelled according to the classification used by Mack (1976). The cancellation effects can be clearly seen in the large expansion coefficients associated with the higher modes. Note that the initial energy is smaller than even the energy of the least-stable OS-mode for this wavenumber combination. If the modes were orthogonal the sum of the squares of the expansion coefficients shown in table 2 would equal unity, i.e. they would add up to the total energy in the associated Fourier component. That sum is here orders of magnitude larger than unity. The largest expansion coefficients for the OS and SQ modes are found in the forks of the A, P and S branches of the respective eigenvalue spectra. The modes in this region depart most from orthogonality, which implies that they have the largest potential for cancellation effects.

The departure from orthogonality is here naturally measured in the inner product associated with the energy norm. It is also remarkable that modes with damping rates

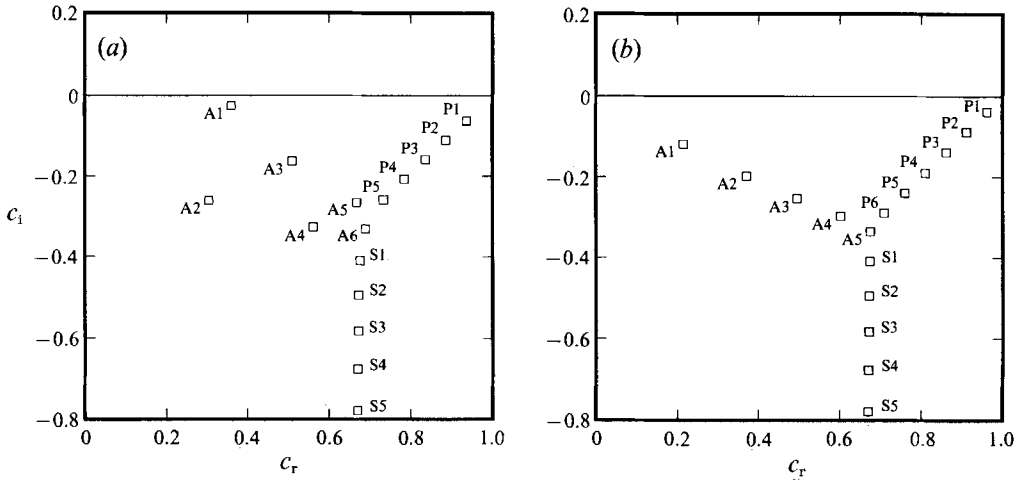

FIGURE 7. (*a*) Orr–Sommerfeld and (*b*) Squire eigenvalues for plane Poiseuille flow with $\alpha = \beta = 1.0472$ and $R = 3000$.

Mode	$\lvert K_l\rvert/E_{\alpha\beta}^{\frac{1}{2}}$	Type	$\lvert B_j\rvert/E_{\alpha\beta}^{\frac{1}{2}}$	Type
1	1.321	A1	0.654	P1
2	0.056	P1	1.466	P2
3	0.182	P2	0.447	A1
4	0.662	P3	3.418	P3
5	6.470	A3	8.022	P4
6	2.529	P4	2.350	A2
7	8.883	P5	18.702	P5
8	0.365	A2	6.055	A3
9	40.567	A5	40.056	P6
10	3.341	A4	35.012	A4
11	3.892	A6	25.118	A5
12	1.223	S1	3.025	S1
13	1.082	S2	0.819	S2
14	0.603	S3	0.416	S3
15	0.399	S4	0.291	S4
16	0.270	S5	0.200	S5
17	0.180	S6	0.132	S6
18	0.119	S7	0.085	S7
19	0.079	S8	0.054	S8
20	0.054	S9	0.035	S9

TABLE 2. Absolute value of the expansion coefficients for the OS and SQ modes at $\alpha = \beta = 1.0472$ and $R = 3000$. The coefficients are normalized with the square root of the initial energy in this wavenumber combination ($E_{\alpha\beta}$). The eigenfunctions are normalized to each have unit energy and they are numbered in order of decreasing imaginary part of their respective eigenvalue. Each mode is also classified according to Mack (1976).

lower that -0.8 are needed to capture the first few time units of the disturbance development. Only sixteen modes are shown in figure 7 whereas twenty modes were needed for a converged initial normal vorticity. Finally, the reason that the transient growth phase of the disturbance development is not mode-like is clearly illustrated by the mode excitation example. The y-dependence of any single mode does not give any information about the y-dependence of the early stages of the disturbance. Instead it

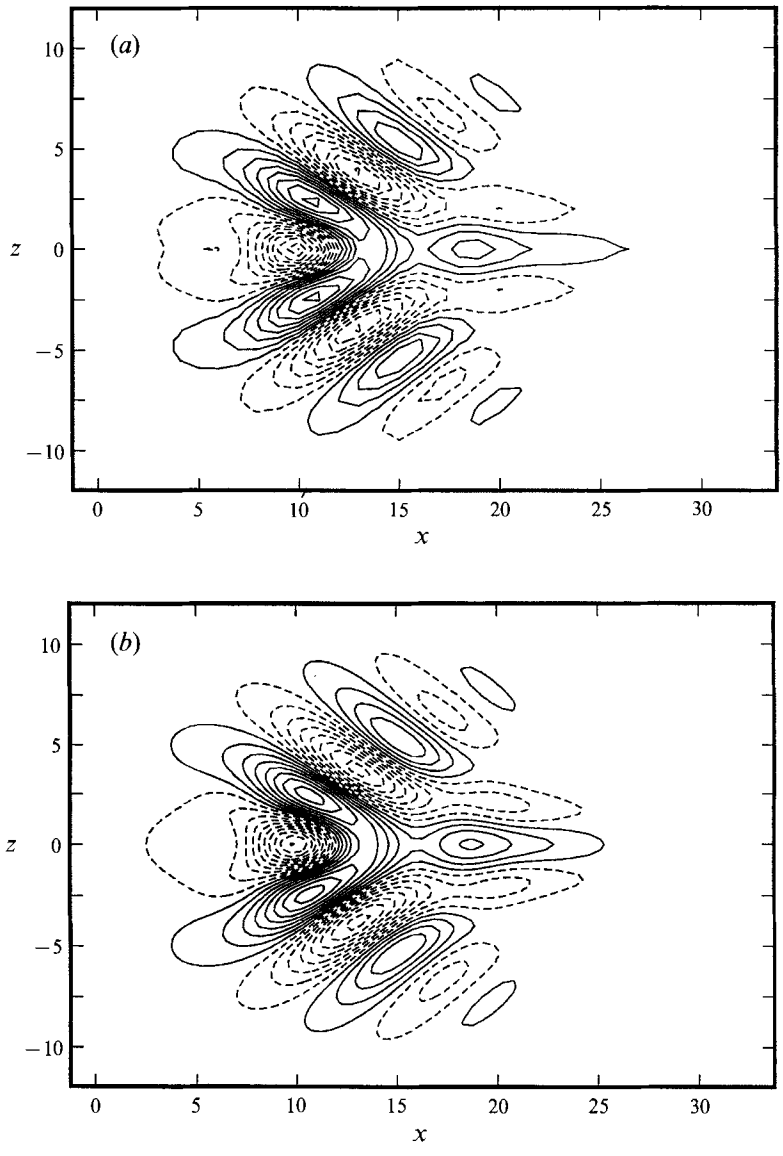

FIGURE 8. Normal velocity at $y = -0.56$ and $t = 30$ of the localized disturbance with $\theta = 0$. (*a*) From eigenfunction expansion using A1-modes only. (*b*) Numerical simulation results. Contour spacing 5.0×10^{-7}.

is determined by a sum of the shapes of the modes with the largest coefficients. In that sum large cancellations occur. It is only after the peak when only a few of the least stable modes are important that the behaviour is similar to what one usually associates with the propagation of eigenmodes.

Another issue of interest is the type of behaviour associated with the different OS and SQ modes. As an example we will investigate the most important OS modes excited at $t = 30$. The least-stable mode is labelled A1 in figure 7(*a*). The mode is also referred to as a TS wave. Figure 8(*a*) shows the velocity associated with the A1-modes. At this time they capture all of the qualitative effects of the normal velocity evolution, as can be seen when figure 8(*a*) is compared to the results of the numerical simulation, figure

8(*b*). The reason the agreement is good without including the modes from the P branch of the OS spectrum is that the expansion coefficients for the least-damped P modes are about an order of magnitude lower than that those for the A1 modes (see table 2). If those modes were substantially excited initially, one would be able to see their effects in figure 8(*a*), since they have only slightly larger damping rates than the A1 mode. Thus we find that one may, with the help of the eigenfunction expansion, predict the development of the normal velocity for this disturbance with a small number of OS modes. For the normal vorticity component one finds that more modes are in general needed to describe the development (compare figures 6*a* and 6*b*).

6. Initial nonlinear evolution

6.1. *Direct numerical simulation results*

In the evolution of the moderate-amplitude disturbances the maximum initial v-velocity was chosen as 0.03 (corresponding to $\epsilon = 0.0699$). In general the development of these disturbances exhibits large differences when compared to those of the small-amplitude case. The normal velocity field for $\theta = 0$ is seen in figure 9 to be dominated by narrow elongated patterns. The wave packet seen in the linear evolution is also present, but plays a minor role since its amplitude is much smaller than the much more localized and faster moving central part of the disturbance. The streaks are seen to be associated with sharp spanwise gradients. A fast moving streaky pattern in front of a wave packet was also found by Chambers & Thomas (1983) in their experimental investigation of the initial stages of a turbulent spot in a Blasius boundary layer. Klingmann (1992) also observed the formation of elongated structures associated with strong spanwise shear in the early stages of spot formation in plane Poiseuille flow.

The signs of nonlinearity are first seen in the normal velocity, and later in the horizontal ones through forcing by the v-component. Neither the normal nor the streamwise velocity decay in the moderate-amplitude case, in contrast to the linear case. When the nonlinearity sets in the disturbance development becomes dominated by the large spanwise shear associated with the formation of streaky structures.

The differences between the linear and nonlinear development of the disturbance with $\theta = 20°$ are not as pronounced as for $\theta = 0$ (figures 4 and 10). The streamwise velocity, for example, grows at similar rates in the nonlinear and linear cases. There are smaller spanwise scales introduced in the central part of the nonlinear disturbance for this value of θ as well, although they are not as pronounced as for the $\theta = 0$ disturbance.

In figure 11(*a*) it is seen that the energy growth in the moderate-amplitude case does not show a large variation with θ. The growth for $\theta = 0$ is dramatically increased as compared to the linear case, whereas the growth for $\theta = 45°$ has decreased slightly. The nonlinear effects dominate after about $t = 10$ for the chosen disturbance. At that time the energy for $\theta = 0$ had reached a maximum in the linear case (figure 5*a*), whereas here it continues to increase (figure 11*a*). Figure 11(*b*) shows the energy decomposition for the moderate-amplitude disturbance, and reveals that the Dv term has grown somewhat at the expense of the normal vorticity in comparison with the linear case (figure 5*b*). This results from the stronger normal gradients for the stronger disturbance as compared to the linear case. However, the decomposition in the two cases follows the same general trend, i.e. that the normal vorticity is responsible for the dominating part of the energy.

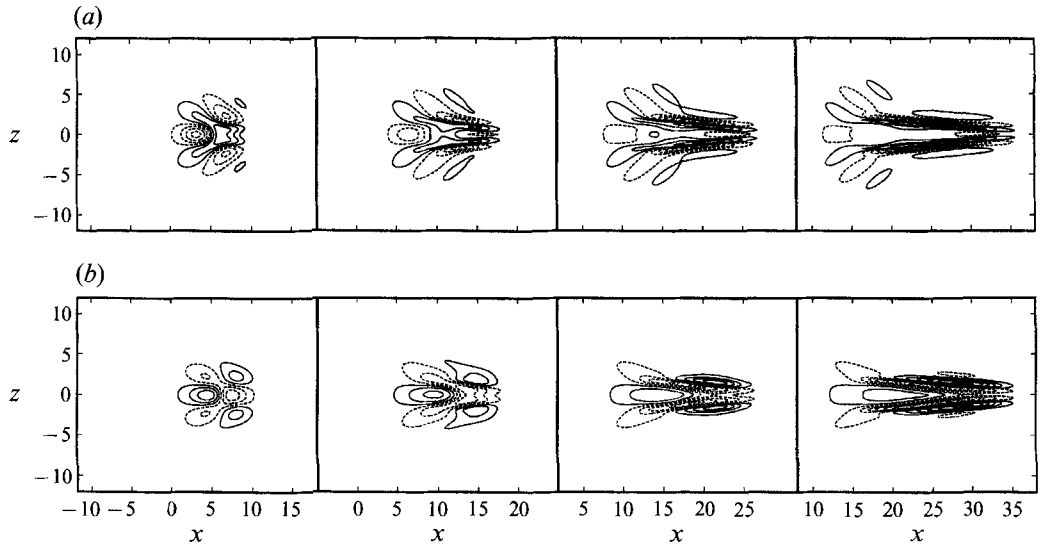

FIGURE 9. Moderate-amplitude disturbance at $y = -0.56$, $\theta = 0$, $t = 10, 20, 30, 40$: (*a*) normal velocity, (*b*) streamwise velocity. Contour spacing: v, 2.5×10^{-3}; u, 2.5×10^{-2}.

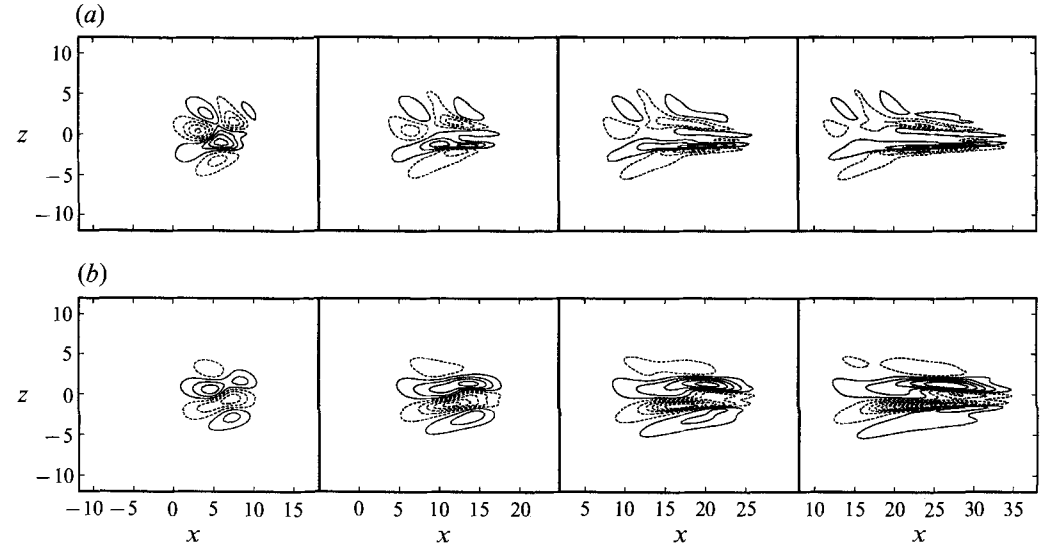

FIGURE 10. Moderate-amplitude disturbance at $y = -0.56$, $\theta = 20$, $t = 10, 20, 30, 40$: (*a*) normal velocity, (*b*) streamwise velocity. Contour spacing: v, 2.5×10^{-3}; u, 2.5×10^{-2}.

6.2. *A numerical amplitude expansion*

In order to study the onset of nonlinearity it is illustrative to analyse the numerical results in terms of an amplitude expansion with the aim of isolating the linear, quadratic and cubic parts of the disturbance. We write the following expansion for the velocity field:

$$u(\epsilon) = \sum_{j=0}^{n} u_k \epsilon^k + O(\epsilon^{n+1}), \tag{20}$$

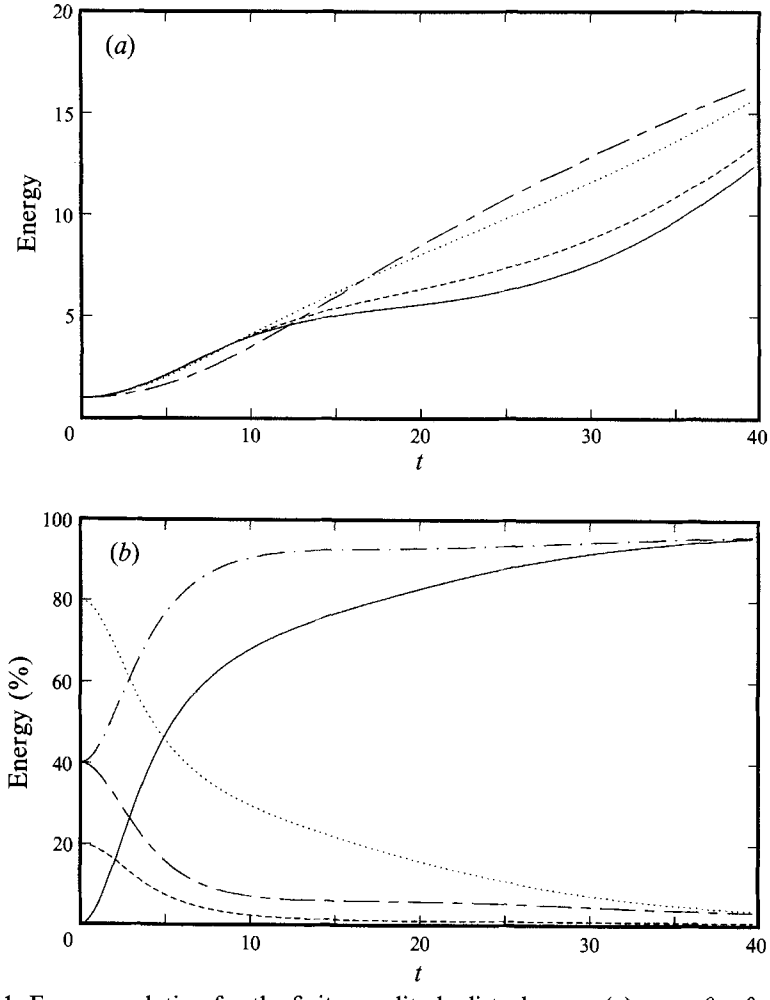

FIGURE 11. Energy evolution for the finite-amplitude disturbances. (*a*) ——, $\theta = 0$; – – –, $\theta = 10°$; · · · · ·, $\theta = 20°$; – · – · –, $\theta = 45°$, normalized by initial energy. (*b*) Percentage contribution from: ——, u; – – –, v; · · · · · ·, w; – · – · –, Dv; – · – · –, η.

where u may represent any of the velocity or vorticity components and where the dependence of x, y, z, t has not been explicitly indicated. In the above expansion we can set $u_0 = 0$ since that represents the parabolic mean flow. The rest of the u_k components can be found by evaluating $u(\epsilon)$ for various values of ϵ and then inverting the expansion (20), neglecting the error term. Assuming that we have used three different values of ϵ we may, at a given time, calculate u_1, u_2, u_3 as solutions to the following linear system

$$\begin{bmatrix} \epsilon_1 & \epsilon_1^2 & \epsilon_1^3 \\ \epsilon_2 & \epsilon_2^2 & \epsilon_2^3 \\ \epsilon_3 & \epsilon_3^2 & \epsilon_3^3 \end{bmatrix} \begin{bmatrix} u_1 \\ u_2 \\ u_3 \end{bmatrix} = \begin{bmatrix} u(\epsilon_1) \\ u(\epsilon_2) \\ u(\epsilon_3) \end{bmatrix}. \tag{21}$$

In our case we chose $\epsilon_1 = 0.0005$, $\epsilon_2 = 0.001$ and $\epsilon_3 = 0.002$ in the disturbance (1) with $\theta = 0$. This system has to be solved for each combination of x, y, z, t of interest.

Figure 12(*a–c*) shows the linear, quadratic and cubic part of the normal velocity in the (x, y)-symmetry plane. The nonlinear parts can be seen to be concentrated to a

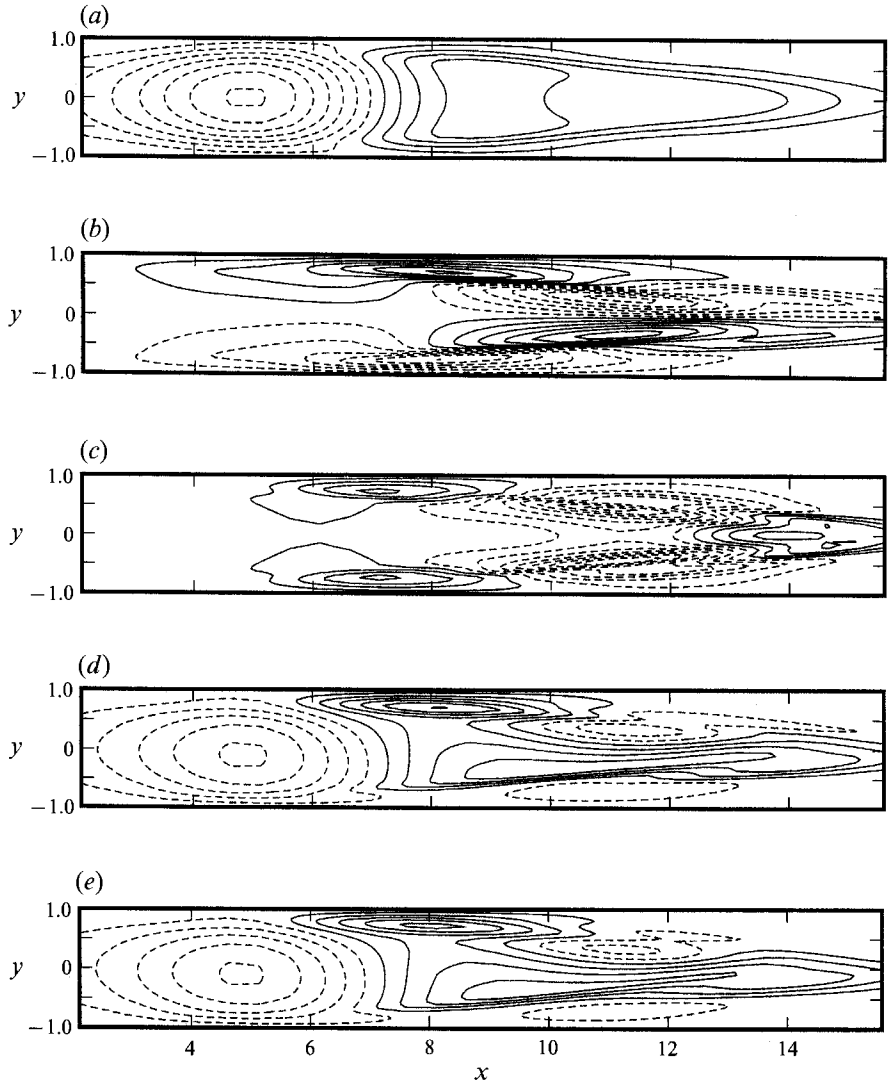

FIGURE 12. Normal velocity at $t = 15$ and $z = 0$. (*a*) Linear part, contour spacing 0.02. (*b*) Quadratic part, contour spacing 0.2. (*c*) Cubic part, contour spacing 2.0. (*d*) Combination of the linear, quadratic and cubic parts. $\epsilon = 0.0699$ with contour spacing 0.002. (*e*) Numerical simulation with $\epsilon = 0.0699$, contour spacing 0.002.

smaller region as well as to have their largest amplitudes closer to the walls. When the initial normal velocity is symmetric in y it is easily verified that the quadratic part will be antisymmetric and the cubic symmetric. Although these symmetries have not been imposed in the calculation of the expansion coefficients they are clearly seen in figure 12(*a–c*), verifying that the rounding and truncation errors have not corrupted the decomposition. Figure 12(*d, e*) compares the sum of the first three terms of the amplitude expansion using $\epsilon = 0.0699$ with the results from the numerical simulation with that amplitude. The agreement is seen to be very good, thus showing that the expansion is valid for substantially higher amplitudes than that used in the calculation of the individual terms. This is further substantiated by the results shown in figure 13, where it is seen that the expansion truncated at third order captures all of the energy

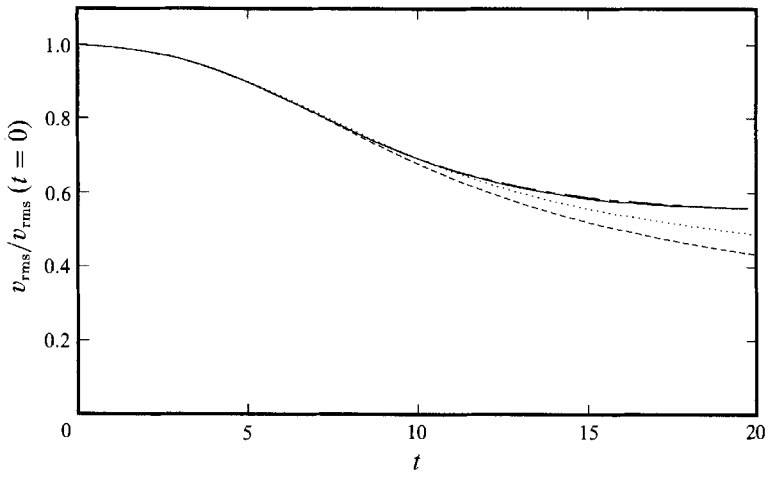

FIGURE 13. Comparison between the v_{rms} obtained from the numerical simulation (——) and the amplitude expansion: – – –, ϵv_1; · · · · · ·, $\epsilon v_1+\epsilon^2 v_2$; – · – · –, (coinciding with the solid): $\epsilon v_1+\epsilon^2 v_2+\epsilon^3 v_3$, where $\epsilon = 0.0699$.

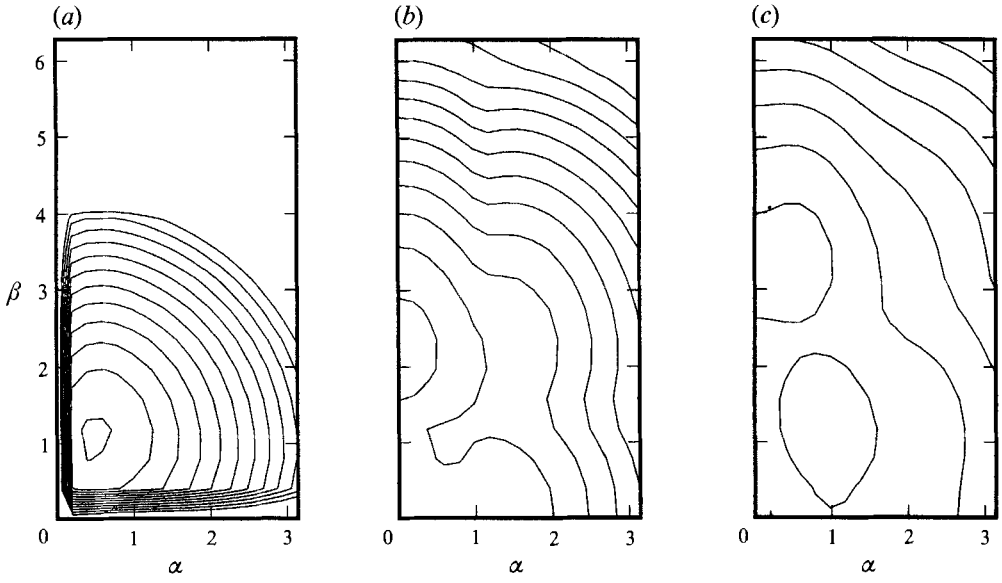

FIGURE 14. Energy spectra at $t = 15$ obtained from the amplitude expansion. (*a*) Linear part. (*b*) Quadratic part. (*c*) Cubic part. Contour spacing 1 decade.

in the normal velocity component up to $t \approx 20$, whereas lower-order truncations deviate from the exact solution at earlier times. The convergence for the horizontal velocity components is not as regular as for the normal velocity, although at $t = 15$ the cubic truncation is sufficient.

The nature of the nonlinear parts is further illustrated in figure 14 where the energy spectra of the first three terms of the expansion are plotted. The quadratic part of the spectrum has peaks along the streamwise and spanwise wavenumber axes, and the cubic term continues the cascade of energy, to smaller spanwise scales, close to the β-axis. Figure 15 shows the three first terms of the streamwise velocity in a (x, z)-plane

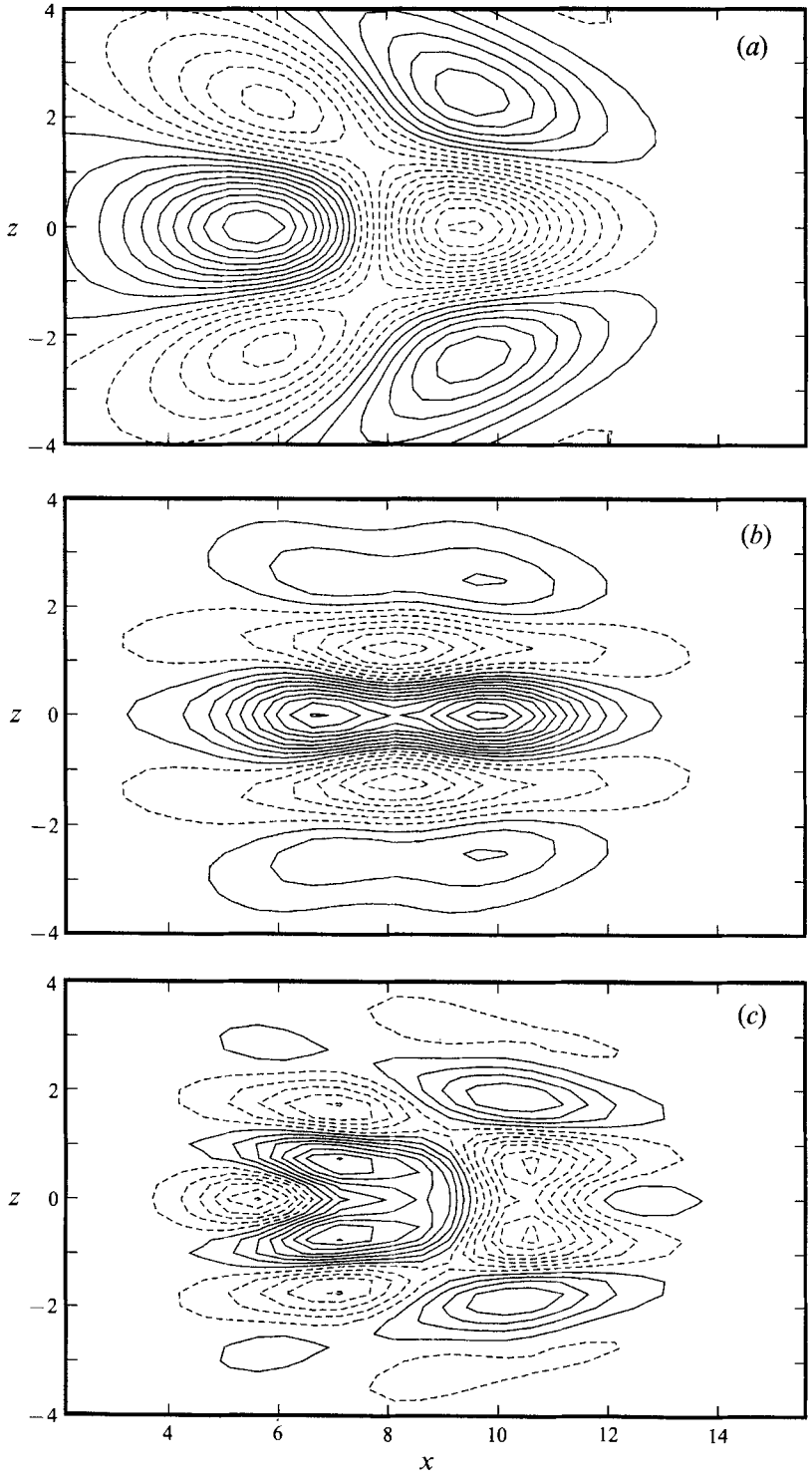

FIGURE 15. Streamwise disturbance velocity at $t = 15$ and $y = -0.707$. (*a*) Linear part, contour spacing 0.1. (*b*) Quadratic part, contour spacing 1.0. (*c*) Cubic part, contour spacing 5.0.

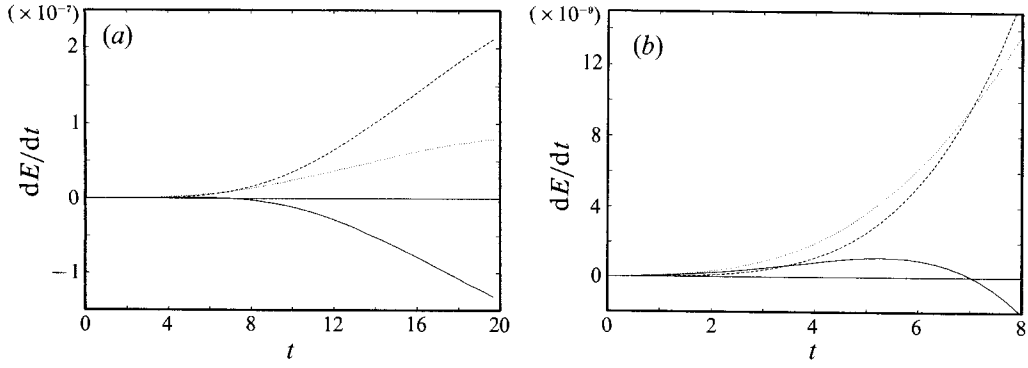

FIGURE 16. Energy transfer into Fourier component (0, 2.36) for the disturbance with $\theta = 0$. (*a*) Up to $t = 20$. (*b*) Enlargement of the initial transfer. ——, Transfer due to nonlinear terms; – – –, transfer due to the linear term; · · · · · ·, total transfer.

obtained from the expansion. The linear part is dominated by the wave packet and the central shear layer, whereas the quadratic part shows the typical streaky structures associated with energy along the spanwise wavenumber axis. The cubic term shows a reinforcement of the shear layer as well as the introduction of smaller spatial scales.

The initial finite-amplitude development can be understood if the nonlinear term of the Navier–Stokes equation is considered. In Fourier space it results in pairwise wavenumber summations seen in the convolution sums in (5). This implies that an initial energy distribution with peaks at $(\pm\alpha, \pm\beta)$ in the spectral plane will give rise to new peaks at $(\pm 2\alpha, \pm 2\beta)$, $(\pm 2\alpha, 0)$, $(0, \pm 2\beta)$ and $(0, 0)$. The last is a modification of the mean profile and the first tends to vanish due to the large values of the exponential damping in that region of wavenumber space. Of the remaining two peaks, the one with zero streamwise wavenumber dominated for the present disturbance. This explains the tendency for formation of elongated patterns with roughly half the wavelength of the initial disturbance. Given the dominance of the zero streamwise wavenumber, first- and higher-order nonlinear interactions tend to shift energy up the β-axis to $(0, \pm 2\beta)$ and further to $(\pm\alpha, \pm 3\beta)$, $(0, \pm 4\beta)$ etc. We will refer to this preferred propagation of energy up the spanwise wavenumber axis as the *β-cascade*.

It may be tempting to attribute the growth of the zero streamwise wavenumber components to the linear effects described in previous sections. One has to remember, however, that these modes are now a solution to a driven problem where the role of the linear mechanism is not obvious. In order to isolate the mechanism behind the rapid growth of these modes the contributions from the linear and nonlinear terms to the energy transfer into the Fourier component (0, 2.36) was calculated using (11). That component is located at the peak of the nonlinearly induced maximum seen in figure 14(*b*). The result is plotted in figure 16. It is clearly seen that it is the linear mechanism that totally dominates the positive energy transfer. The major effect of the nonlinear terms is to remove a substantial amount of the energy supplied by the linear mechanism. Since this Fourier component has no energy initially for the $\theta = 0$ disturbance it needs to be nonlinearly excited. An enlargement of the initial transfer shows that this is indeed the case (figure 16*b*). Thus after a small nonlinear excitation all of the energy supplied to the flow for this Fourier component is due to the linear mechanism. One should note that the above reasoning is valid also for small non-zero streamwise wavenumbers (see (19) and the subsequent discussion).

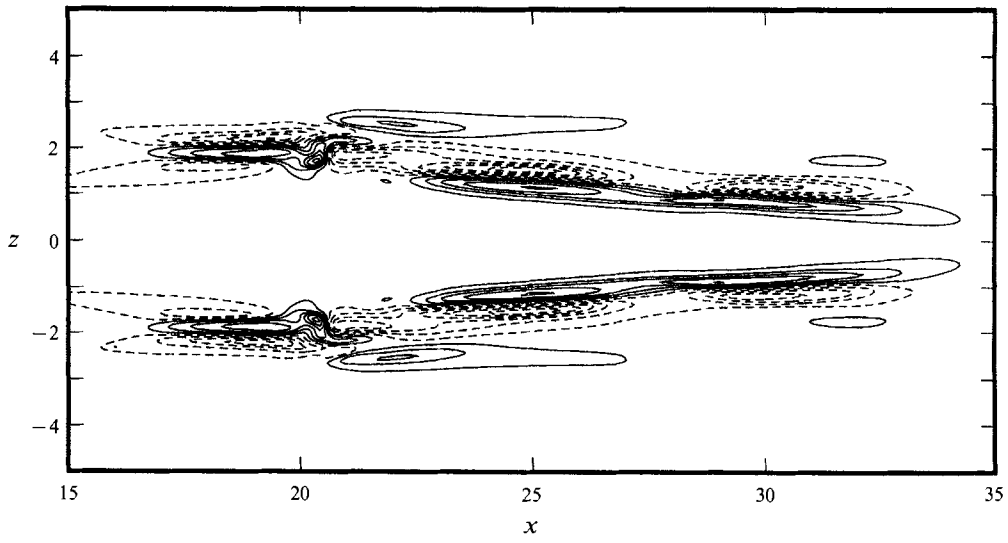

FIGURE 17. Large-amplitude disturbance at $t = 40$ and $y = -0.56$. Normal velocity, contour spacing 0.02.

7. Strong nonlinearity and breakdown to turbulence

In order to facilitate the study of breakdown to turbulence from localized disturbances the initial amplitude was raised to 6% (corresponding to $\epsilon = 0.1399$). By this increase in amplitude the development reaches the stage of a small turbulent spot after a relatively short time ($t \approx 60$).

Before we consider the breakdown we will briefly compare the flow features of the 6% disturbance with that of the previously discussed finite-amplitude disturbance. The normal velocity at $t = 40$ (figure 17) shows the same streaky structure as for the lower amplitude in figure 9. Note that the region plotted in figure 17 is smaller than that in the figures from the lower-amplitude disturbances, so that the wave packet behind the streaky part cannot be seen. On closer inspection one finds some significant differences. For the lower amplitude the streaky structures are smooth and extend over a streamwise length of about 20. For the corresponding higher amplitude they are instead broken up into two substructures, one from 15 to 20 and one from 22 to 35. In between there is a spanwise shift of the streaks. We here focus on the description of the streaky pattern at the rear of the disturbance in the lower half of the channel, since the subsequent breakdown was found to originate there. Figure 18 shows the streamwise vorticity in the three (y, z)-planes in this region. A prominent feature are the strong streamwise vortices situated close to both the upper and lower walls, which in turn are associated with inclined vertical shear layers (see figure 19*a*). At the lower wall a twisted vortex pair is found between $x = 17$ and 20 whereas the main feature further downstream is a single strong vortex with the dominating component in the streamwise direction. Such a slightly inclined vortex in a shear flow becomes intensified by the action of the mean shear. When nonlinear and viscous terms are neglected the equation for the streamwise vorticity component (ξ) becomes

$$\mathrm{D}\xi/\mathrm{D}t = U'(\eta - \partial u/\partial z) \tag{22}$$

where $\mathrm{D}/\mathrm{D}t$ denotes material derivative.

At $t = 40$ the breakdown of the streamwise vortex structure is just starting. It can be seen as a small kink in the streamwise velocity contours in figure 19(*a*). In an

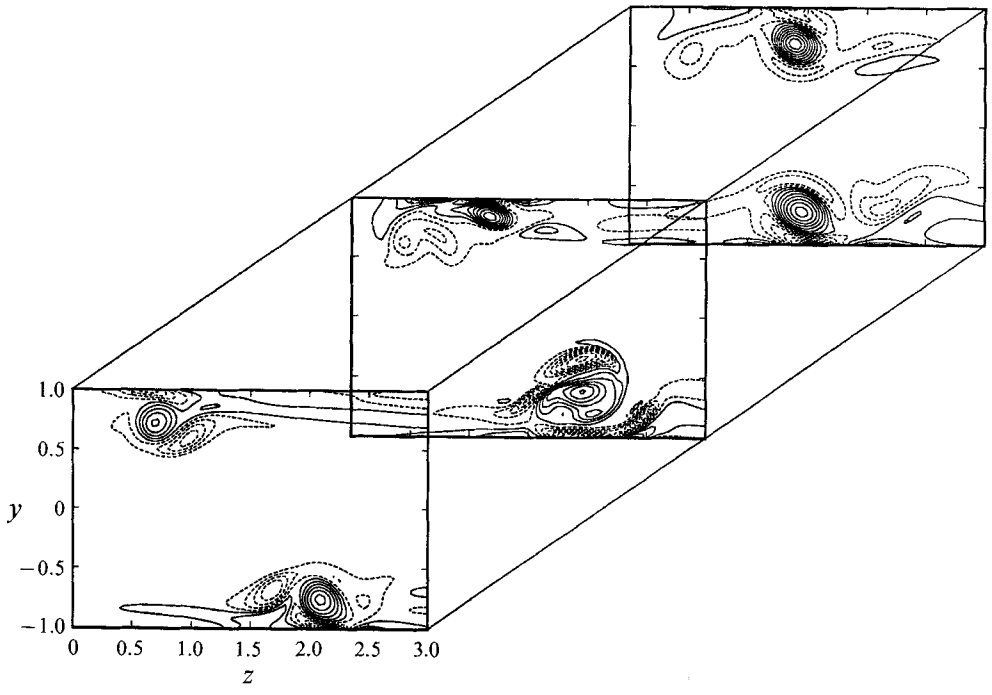

FIGURE 18. Large-amplitude disturbance at $t = 40$. Streamwise vorticity at $x = 17, 20, 23$. Contour spacing 0.25.

experiment where a velocity component is measured with a fixed probe this will appear as a sharp spike in the signal. This is the start of a rollup process, clearly seen at $t = 45$ in figure 19(*b*). The shear layer associated with the vortex rolls up in a manner similar to that accompanying the lambda vortex structures in the secondary instability process. The initiation of the breakdown is quite local in both space and time, which is illustrated by the evolution of the normal velocity between $t = 40$ and 45. The maximum v grows rapidly up to a magnitude of about 0.2 during this period. The region with high values of the normal velocity has a length of about one unit, to be compared with the vortex structures, which are an order of magnitude longer.

After the spike stage the flow quickly breaks down and forms a turbulent spot. The normal velocity at $t = 64.2$ can be seen in figure 20. Here the rear part of the disturbance already has the forward pointing arrowhead typical of early channel flow spots (Alavyoon, Henningson & Alfredsson 1986). Notice that the front part of the disturbance has much lower amplitudes than the region which has broken down. This faster moving part vanishes as the disturbance propagates forward and turns into a fully developed spot. The propagation velocity of the rear laminar–turbulent interface was found to be 0.55 ± 0.1, well in accordance with previous experimental and numerical findings. See Henningson & Kim (1991) for further details on the Poiseuille flow spot. The box size is here too small, however, to follow the disturbance much further.

8. Discussion of the generality of the transition process

We have described a transition scenario for a particular class of localized disturbances in plane Poiseuille flow. An essentially linear mechanism was found to be important for the rapid growth of the disturbance both for small and large initial

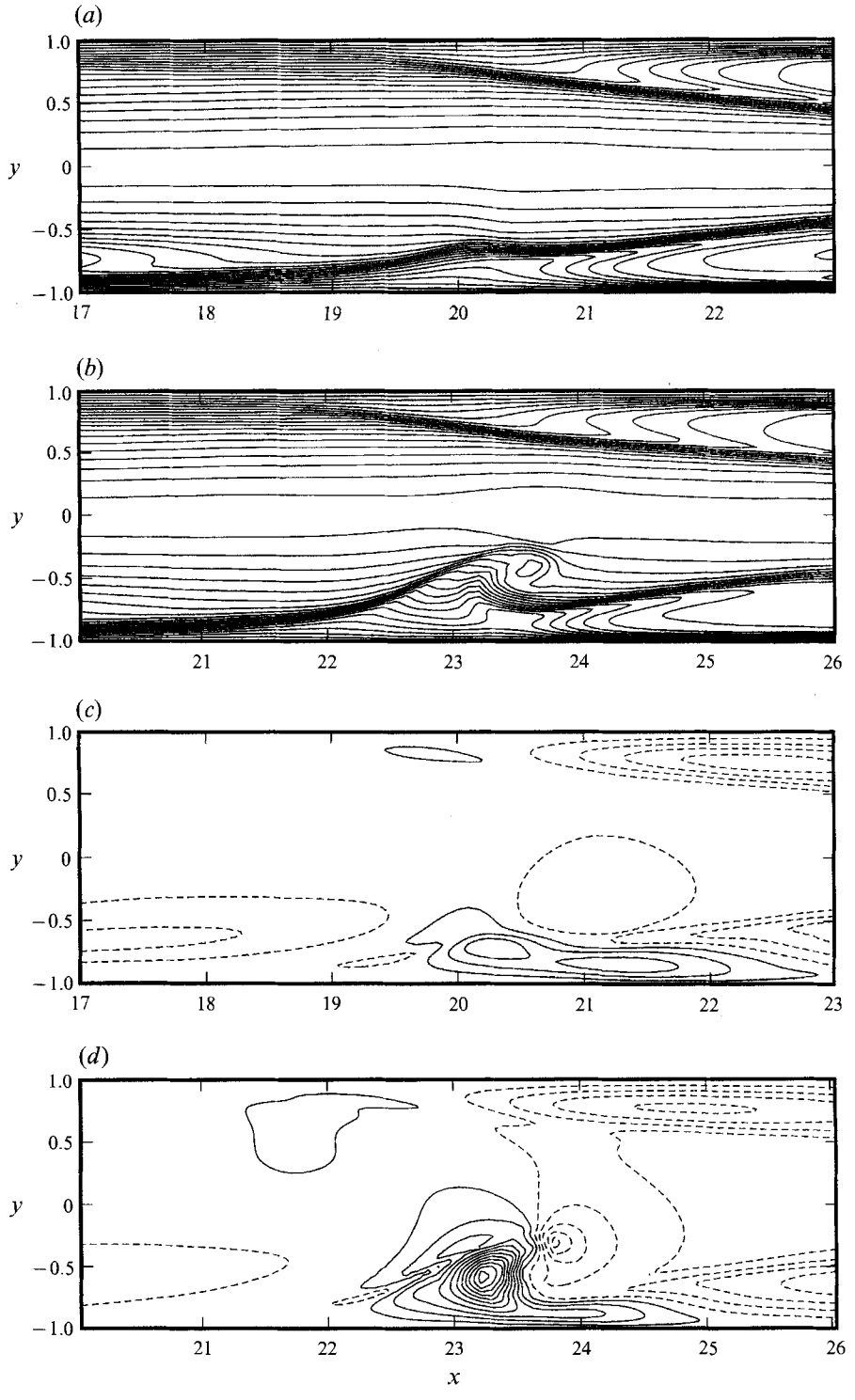

FIGURE 19. Strong disturbance for $z = 1.5$. (*a*) Streamwise velocity at $t = 40$, contour spacing 0.05. (*b*) Streamwise velocity at $t = 45$, contour spacing 0.05. (*c*) Normal velocity at $t = 40$, contour spacing 0.02. (*d*) Normal velocity at $t = 45$, contour spacing 0.02.

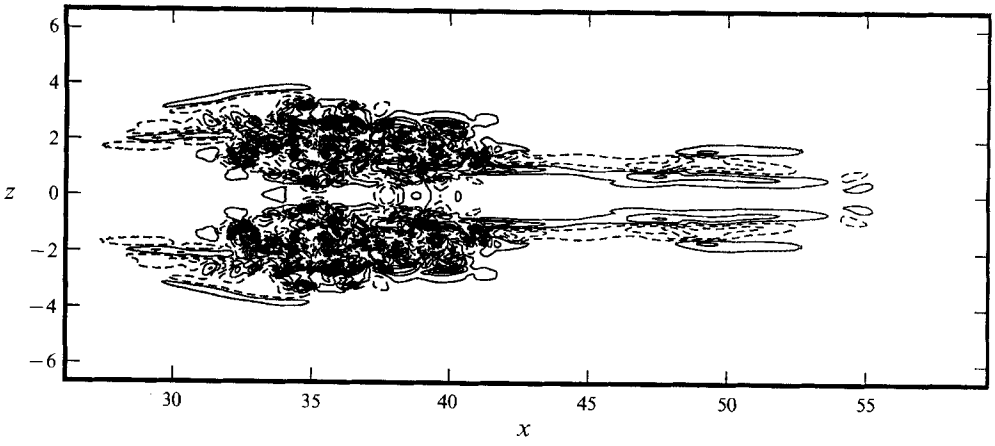

FIGURE 20. Normal velocity at $t = 64.2$ and $y = -0.56$, contour spacing 0.025.

amplitudes. The question that naturally arises is whether this represents a scenario that is present for other disturbances and flow situations. We will here address the question of the generality of this mechanism. First another kind of disturbance, distinctly different from that treated in the previous sections, is considered in plane Poiseuille flow whereafter localized disturbances in the boundary-layer geometry are discussed. We will focus on the generality of the streak formation and the development of the strong streamwise vortex structure. The later stages of breakdown require such large amounts of computer time that a detailed parameter study and comparison with other flow situations are outside the scope of this study.

8.1. *An axisymmetric disturbance in Poiseuille flow*

A disturbance consisting of an axisymmetric vortex given by (3*b*) is considered in the present section. Axisymmetric disturbances with their symmetry line parallel to the normal direction have zero normal vorticity. More importantly, the energy of such disturbances in Fourier space has a qualitatively different distribution than the disturbances previously considered. It is easy to show that horizontal axisymmetry also implies axisymmetry in wavenumber space. The particular disturbance used here has a maximum of initial energy at a radius of about $k = (\alpha^2+\beta^2)^{\frac{1}{2}} = 0.8$ in Fourier space. The energy is zero at the origin and drops rapidly for large values of k. Thus this disturbance has a sizable amount of energy near the spanwise wavenumber axis, while the peaks at specific wavenumber combinations associated with the previously used disturbances are absent. Finally the disturbance, in contrast to those studied above, lacks the symmetry in the normal direction.

The development of this disturbance exhibits the familiar wave packet structure in v at the rear of the disturbance as well as a streaky structure at the front. Figure 21 shows the normal and the streamwise velocity at $t = 30$ for the moderate initial amplitude ($\epsilon = 0.0138$). The streamwise velocity is also developing a streaky structure. The energy has grown by a factor of approximately 15 during the first 30 time units.

The features described are similar to the $\theta = 20°$ disturbance seen in figure 9. In order to determine whether the mechanism generating the growth is similar we will perform the numerical amplitude expansion previously done for the $\theta = 0$ disturbance. We use the same three values of ϵ and solve the system (21) at each grid point for $t = 15$. The energy spectra of the linear, quadratic and cubic terms obtained using this procedure are seen in figure 22. The linear spectrum has now lost is initial axisymmetry

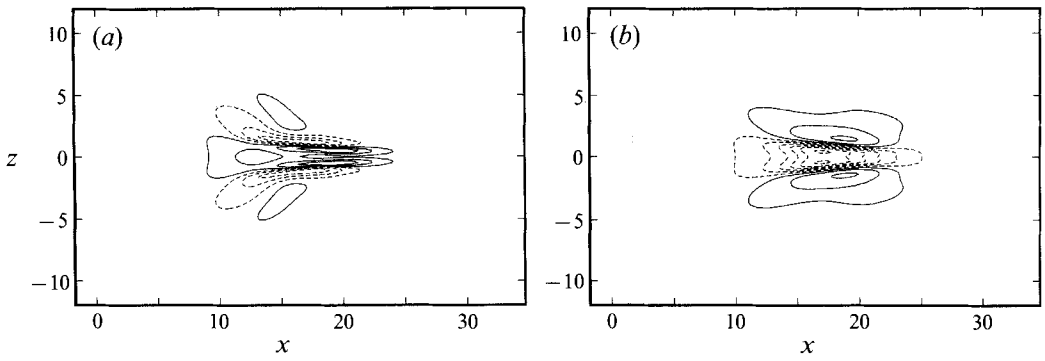

FIGURE 21. Normal velocity for the moderate-amplitude axisymmetric disturbance with $\epsilon = 0.0138$ at $t = 30$ and $y = -0.56$. (*a*) Normal velocity, (*b*) streamwise velocity. Contour spacing 2.5×10^{-3} for the normal velocity and 2.5×10^{-2} for the streamwise velocity.

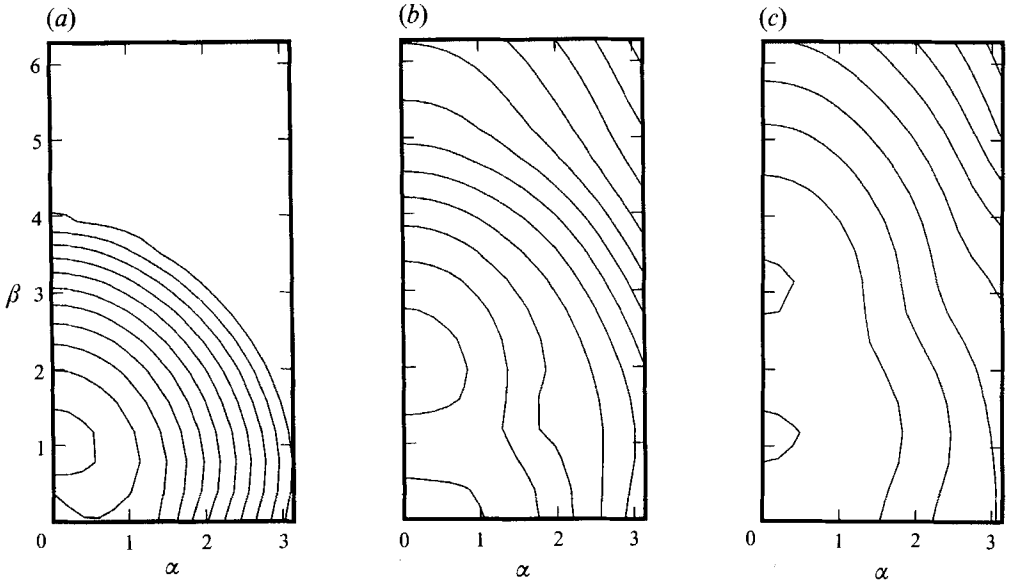

FIGURE 22. Energy spectra at $t = 15$ obtained from the amplitude expansion of the axisymmetric disturbance. (*a*) Linear part. (*b*) Quadratic part. (*c*) Cubic part. Contour spacing 1 decade.

and instead has most of the energy concentrated around the spanwise wavenumber axis. This is again due to the transient growth experienced by the normal vorticity in this region of wavenumber space. The quadratic and cubic spectra show that the initial nonlinear interactions propagate the energy up the spanwise wavenumber axis. This is similar to the β-cascade seen for the $\theta = 0$ disturbance. Note that the streaks generated by the quadratic term have a spanwise scale half of that of the linear streaks and can be most clearly seen in the normal velocity (figure 21 *a*), since that velocity component does not have a large growth caused by the linear mechanism. The streamwise velocity, on the other hand, is dominated by the growth associated with the linear term.

In addition to having qualitatively the same initial nonlinear interactions and streak formation process as the initial disturbance with counter-rotating vortices, the large-amplitude axisymmetric disturbance also develops distinct and strong streamwise vortices. Figure 23 shows the streamwise vorticity in a (y, z)-plane. A strong

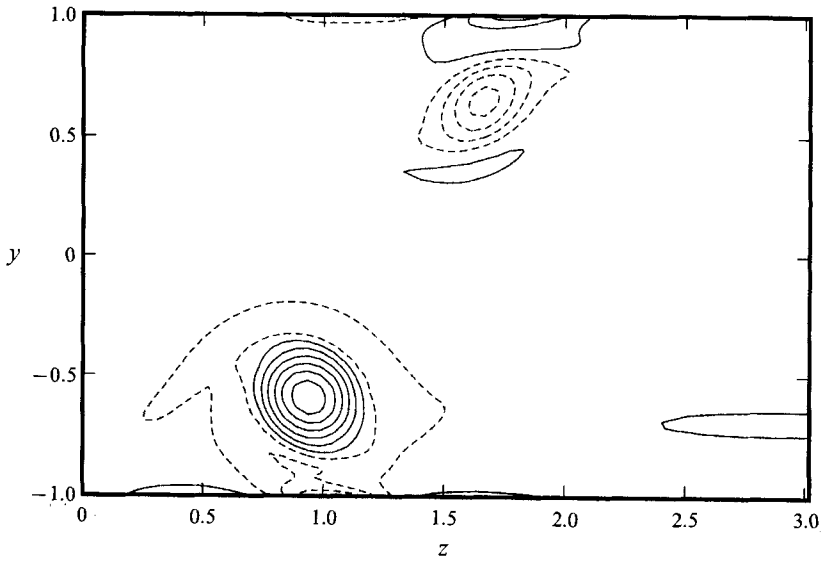

FIGURE 23. Streamwise vorticity at $x = 23$ and $t = 40$ obtained from the large-amplitude axisymmetric disturbance ($\epsilon = 0.0276$). Contour spacing 0.25.

streamwise vortex has developed at the bottom of the channel with a strength comparable to that seen in figure 18. Here it is only seen at the bottom of the channel, however. This is most likely a result of the asymmetric initial amplitude of the disturbance in the normal direction in which most of the perturbation energy is located in the bottom half of the channel.

8.2. *Comparison with the boundary-layer case*

The linear development of a localized disturbance in a Blasius boundary-layer flow may be expected to differ somewhat from the Poiseuille case, owing to the different linear stability characteristics of the two flows. The linear critical Reynolds number, based on the maximum velocity and the displacement thickness δ_*, is about 500 for the Blasius flow and 1900 for the Poiseuille flow. At equal Re_{δ_*} the wave packet thus can be expected to be more important in the boundary layer, at least for long times.

Breuer & Landahl (1990) investigated the development of disturbances with a low but finite amplitude in Blasius flow at $Re_{\delta_*} = 950$ and observed the nonlinear generation of streaks. This Reynolds number is practically identical to the one in the present Poiseuille flow study ($Re_{\delta_*} = 1000$). The observations of Breuer & Landahl are however quite different from the present findings. They found that the inclined shear layer that forms in the central part of the disturbance experiences a secondary instability dominated by two-dimensional ($\beta = 0$) modes of high wavenumber. This secondary instability was found to be completely confined to the central portion of the disturbance.

To investigate this discrepancy, the boundary-layer simulations of Breuer & Landahl were here repeated with particular emphasis on possible effects of insufficient spatial resolution. It was found that the secondary instability observed by Breuer & Landahl is a numerical artifact induced by insufficient resolution in the wall normal direction (see for example figure 3, $t = 117$ in that paper). In figure 24(*a*) the numerical instability is shown to appear when 33 spectral modes were used in the y-direction. This instability vanishes completely when twice that number of modes were used as seen in figure 24(*b*). A further increase of the number of modes in the y-direction to 97 and

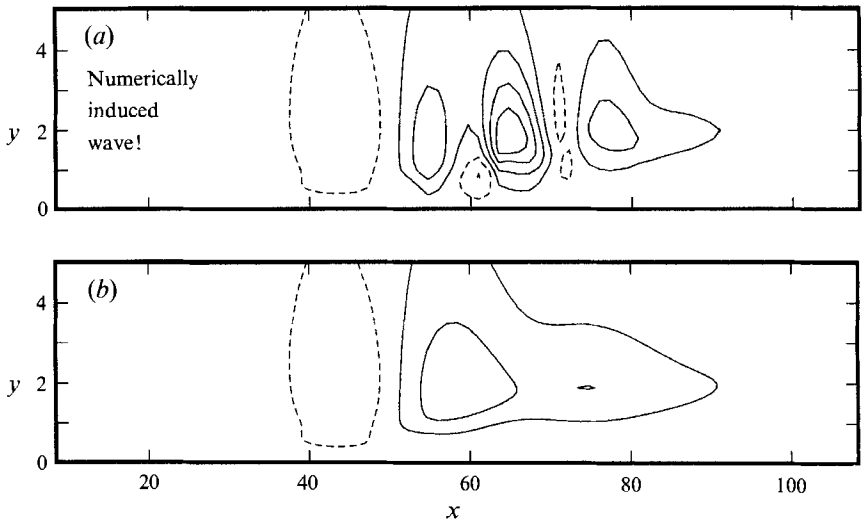

FIGURE 24. Normal velocity for the finite-amplitude disturbance in the boundary layer at $t = 117$, $z = 0$ with normal resolution: (*a*) 33 modes, (*b*) 65 modes. The time and spatial coordinates are here scaled with δ_* and the free-stream velocity. Contour spacing is in both cases 0.002.

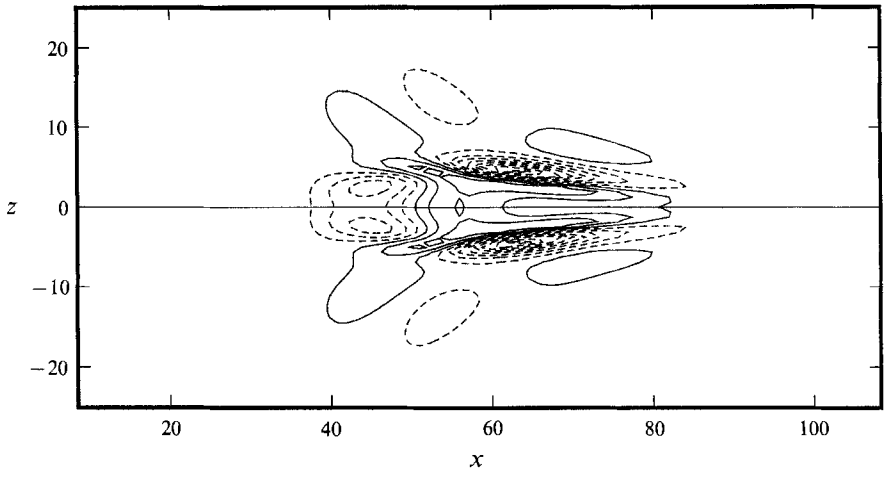

FIGURE 25. Normal velocity for the finite-amplitude disturbance in a boundary layer at $t = 117$, $y = 0.99$. The time and spatial coordinates are here scaled with δ_* and the free-stream velocity. Contour spacing is 0.001.

increase of the resolution in the two other directions gave differences only slightly larger than the precision of the graphics, showing that these results are numerically converged. The strength of the numerical instability could be arbitrarily varied with the resolution in the normal direction. Tests showed that the presented results are unaffected by the vertical extent of the computational domain as long as it exceeds $3\delta_*$. The effect of boundary-layer growth was also investigated and it was found that even a complete suppression of the growth gave only minor changes in the solution. Finally a simulation with a non-parallel boundary layer was performed and again the solution was essentially unaffected.

Indeed the streak formation in the boundary layer (figure 25) is qualitatively the same as that in the Poiseuille flow (figure 9, $t = 40$). Note that $t = 40$ corresponds to

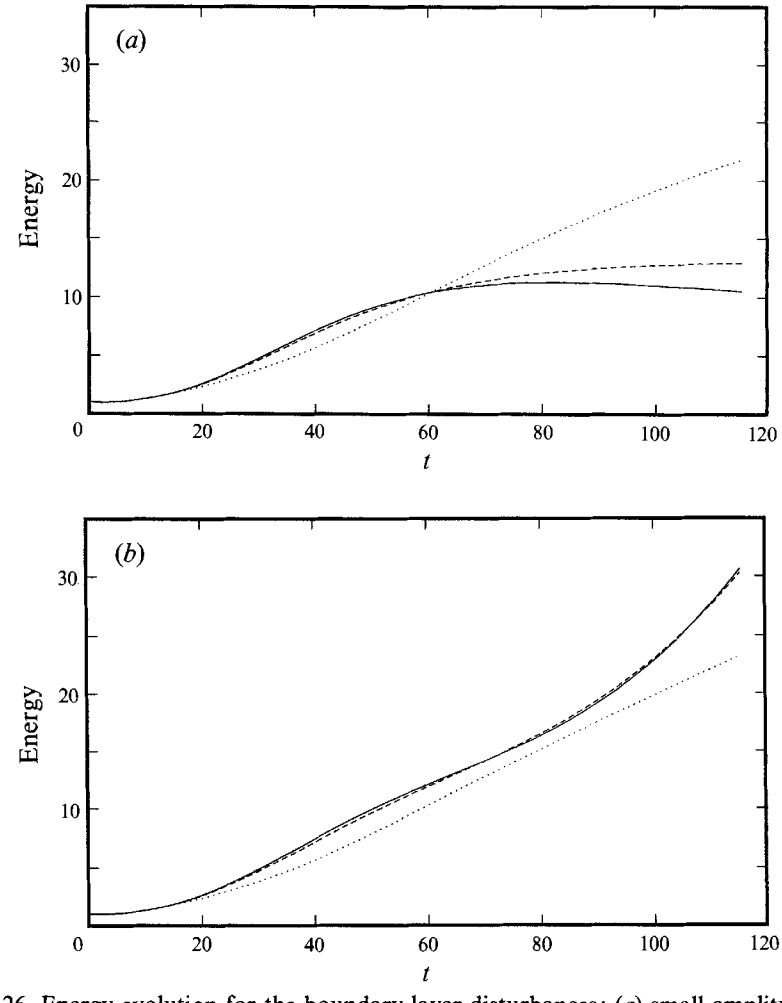

FIGURE 26. Energy evolution for the boundary-layer disturbances: (*a*) small-amplitude disturbance ($\epsilon = 0.001$); (*b*) moderate-amplitude disturbance ($\epsilon = 0.2$): ——, $\theta = 0$; – – –, $\theta = 10°$; · · · · · ·, $\theta = 45°$; normalized by initial energy.

120 if scaled with δ_*, and that the boundary-layer disturbance has an initial maximum normal velocity which is about five times lower than the normal velocity for the moderate-amplitude Poiseuille disturbance.

To further substantiate the similarity of the Poiseuille and boundary-layer cases, asymmetric ($\theta \neq 0$) disturbances were also considered in the boundary-layer flow. Figure 26 shows the evolution of total disturbance energy in the boundary layer for various values of θ, both for small and moderate amplitudes. The behaviour is seen to be similar to the Poiseuille case (figures 5*a* and 11*a*) with the growth increasing with increasing rotation angle of the initial disturbance for the small-amplitude disturbances. For $\theta = 0$ the amplitude has just started to decrease by the end of the simulation. This difference from the marked decay in the corresponding Poiseuille flow simulation is most likely a result of low damping or even growth at this supercritical Reynolds number of several wave components which have small β/α. A subcritical boundary-layer simulation would give results resembling more closely the Poiseuille case. In both flows the spread in amplitude growth is much smaller in the moderate-

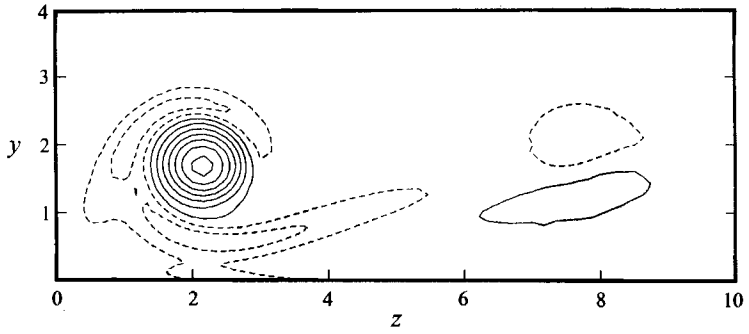

FIGURE 27. Streamwise vorticity at $x = 75$ and $t = 117$ obtained from the large-amplitude disturbance in a boundary layer ($\epsilon = 0.7$). Contour spacing 0.1.

amplitude case. It is plausible to assume that the reason is the same nonlinear excitation of algebraic growth as seen in Poiseuille flow. Finally for a larger amplitude initial disturbance strong streamwise vortices with a circular cross-section develop at a position and with a strength close to that in the Poiseuille flow case (figure 27). Other qualitative flow features of this disturbance are also the same as the corresponding large-amplitude Poiseuille disturbance.

Thus we have seen that localized disturbances in Poiseuille and boundary-layer flow behave in a similar manner. One should note, however, that the instability observed by Breuer & Landahl (1990) arose in conjunction with a shear layer associated with locally inflexional velocity profiles, and hence could intuitively be expected to be physical. To investigate whether the large numerical errors due to the insufficient resolution in their simulation possibly could be equivalent to the effect of free-stream turbulence or other perturbations of the flow and thus could have triggered a physical instability, we added noise to the well-resolved calculations. White wideband noise, spatially evenly distributed with a peak amplitude of 20% of the primary disturbance was used to model the perturbations. First the noise was superimposed on the initial flow field and, in a second simulation, on a flow field at $t = 43$. In neither case did the flow exhibit any instability. In a last effort to try to find an instability, the numerically induced wave packet at $t = 43$ was extracted from the unresolved calculations and added to the converged solution at that time. When the combined flow field was integrated in time the wave packet was found to grow slightly, although with a substantially lower growth rate than in the unresolved calculations.

Although the possibility of a wave packet instability on the shear layer cannot completely be discarded based on these results, it seems highly unlikely that it would be seen in a real flow situation at these low amplitudes. It is well known that a high-amplitude disturbance can generate a lambda vortex structure with an instability resembling the Breuer & Landahl findings in the 'head' of the vortex, see Kovasznay, Komoda & Vasudeva (1962). However, this occurs for a shear layer which is an order of magnitude stronger than in the present case.

9. Conclusions

Transition to turbulence from a localized disturbance was here studied by direct numerical simulations of disturbances with a range of amplitudes, starting from the stages of linear evolution to the final breakdown and formation of a small turbulent spot. Simulations of turbulent spots have previously been reported for Poiseuille,

boundary-layer and plane Couette flow (see Henningson *et al.* 1987; Lundbladh & Johansson 1991). In these studies the growth and spreading characteristics, as well as turbulence statistics have been determined. The present study is focused on the earlier phases of the transition to turbulence and presents the first simulation carried out with sufficient spatial resolution to ensure fully numerically converged solutions for all stages of the breakdown and formation processes. Small-amplitude simulations were also made and compared with results from linear expansions.

It was demonstrated that for the evolution of localized disturbances in Poiseuille and boundary-layer flows, the kinetic energy becomes strongly dominated by the part associated with the normal vorticity generated by the three-dimensional liftup effect. The small-amplitude disturbances were shown to grow essentially algebraically over an increasing length of time with increasing amount of energy in lower streamwise wavenumbers. One should note that the growth in kinetic energy can occur despite decay of all of the eigenmodes. This transient growth is only possible because the eigenmodes are non-orthogonal and is physically due to tilting of the mean spanwise vorticity such that normal disturbance vorticity is created. The small-amplitude disturbances in Poiseuille flow were analysed using an eigenfunction expansion in OS and SQ modes. It was found that the largest transient growth occurred for small streamwise wavenumbers, explaining the emergence of elongated structures in the streamwise direction. The eigenfunction expansion also showed that the initial phases of the growth was not mode-like but dominated by cancellation effects present when a number of non-orthogonal eigenmodes propagate.

For finite amplitudes the nonlinear development becomes dominated by pairwise wavenumber summations that give rise to disturbance components with zero streamwise wavenumber. Once energy was nonlinearly transferred to Fourier modes with zero streamwise wavenumbers it was shown that a linear mechanism caused the large growth seen in these components. These streaky structures rapidly constitute the main part of the disturbance. Thereby, the dependence on the initial amount of energy in low streamwise wavenumbers becomes largely eliminated. The results imply that practically all localized disturbances will develop a streaky horizontal velocity pattern, since energy in low streamwise wavenumbers is in general generated by nonlinear interactions if it is not present initially. These nonlinear interactions also produce increasingly smaller scales. It was further pointed out that the total disturbance energy can only grow due to linear effects. For subcritical flows this means that the transient growth effects analysed in the present paper must operate for transition to take place.

The breakdown stage of the localized disturbances in Poiseuille flow was also analysed. It was shown that a strong streamwise vortex formed on either side of the symmetry plane at $z = 0$. The sharp shear layers associated with the lower vortices were seen to roll up, giving a situation similar to the first spike stage observed in the breakdown of large-amplitude two-dimensional TS waves. After the first sign of breakdown the disturbance quickly developed into a small turbulent spot.

Breuer & Haritonidis (1990) found that a dominating feature of the evolution of small-amplitude localized disturbances in boundary layers is the generation of an inclined shear layer by the liftup effect. This effect was found in the present study to be essentially identical in Poiseuille flow.

The symmetric finite-amplitude disturbances presented here are qualitatively the same as the ones presented by Chambers & Thomas (1983) in their investigation of the early stages of breakdown of localized disturbances in boundary-layer flow. They also found that it is the streaky pattern in front of the wave packet that breaks down and forms a turbulent spot.

Cohen *et al.* (1991) studied a local disturbance in the form of a low-amplitude small air pulse in a supercritical boundary-layer flow. In this situation the initial growth was found to be dominated by that of the two-dimensional TS wave followed by a Craik-type subharmonic resonance. The measured energy spectra after the resonance stage exhibit dominant peaks for oblique waves, which interact to transfer energy to low streamwise wavenumbers in a manner similar to that in the present investigation.

Klingmann (1992) used a substantially stronger disturbance in the form of an air pulse in plane Poiseuille flow at $Re = 1500$. After an initial strongly nonlinear phase she observed a fairly large-scale elongated disturbance. She concluded that the subsequent growth could essentially be explained by linear mechanisms. For higher initial amplitudes she found generation of smaller spanwise scales and subsequent breakdown involving a short spike of length similar to that shown in figure 19 in the present investigation.

Breuer & Landahl (1990) investigated the development of the corresponding finite-amplitude disturbances and observed the nonlinear generation of streaks. However, their results indicated a rather different breakdown scenario from that found in the present study. The discrepancy was here shown to be ascribable to insufficient numerical resolution in their study. High-resolution boundary-layer computations were here carried out, and shown to yield a behaviour in the weakly nonlinear regime quite similar to that for Poiseuille flow.

The results presented here, as well as those of the other investigators discussed above, show that a transition scenario starting with localized disturbances can bypass the growth of two-dimensional TS waves and their secondary instability. It is plausible to assume that excitation of the algebraically growing normal vorticity along the spanwise wavenumber axis is an integral part of the growth mechanism for all of these cases, particularly when the total disturbance energy can only increase due to linear effects.

The prominence of Fourier components with zero streamwise wavenumber has also been noted in compressible simulations of transition on a cone (Pruett & Zang 1992), in simulations of incompressible channel flow starting with random disturbances (Kim & Moser 1989) and in simulations of incompressible boundary layers using the parabolized stability equations (Bertolotti & Herbert 1990). Schmid & Henningson (1992) started with two interacting oblique waves in Poiseuille flow and showed that nonlinearly induced Fourier components with low streamwise wavenumbers generated practically all of the total disturbance growth by the linear mechanism described in the present investigation. These investigations suggests that the essentially linear mechanism described here is operating in a wide variety of flow situations and is not only relevant for the particular transition scenario investigated in this study.

For the disturbances studied here the streamwise vorticity associated with the streaky structures develop into strong vortices if the disturbances is strong enough. The streamwise vortices in turn experience a highly localized and rapid breakdown which quickly results in a turbulent spot. An interesting question is whether this second part of the bypass transition scenario is as general as the nonlinear excitation of transient growth appears to be. These and other key questions will presently be studied in order to yield an improved understanding of this transition mechanism.

We wish to thank Peter Schmid for graciously assisting us with the calculations of the contributions to the energy transfer shown in figure 16. We wish to thank Håkan Gustavsson for fruitful discussions on the topic of localized disturbances. We also wish to thank the referees for constructive critique. We gratefully acknowledge financial

support from the Göran Gustafsson Foundation and the Aeronautical Research Institute of Sweden (FFA). Supercomputer time was provided by the National Center for Supercomputer Applications (NCSA), Urbana, Illinois and the National Supercomputer Center (NSC), Linköping, Sweden. Computations were also carried out at the MIT Supercomputer Facility.

REFERENCES

ALAVYOON, F., HENNINGSON, D. S. & ALFREDSSON, P. H. 1986 Turbulent spots in plane Poiseuille flow – flow visualization. *Phys. Fluids* **29**, 1328–1331.

BAYLY, B. J., ORSZAG, S. A. & HERBERT, T. 1988 Instability mechanisms in shear flow transition. *Ann. Rev. Fluid Mech.* **20**, 359–91.

BERTOLOTTI, F. P. & HERBERT, T. 1990 Fast simulation of boundary-layer transition with PSE. *Bull. Am. Phys. Soc.* **35**, 2230.

BREUER, K. S. & HARITONIDIS, J. H. 1990 The evolution of a localized disturbance in a laminar boundary layer. Part 1. Weak disturbances. *J. Fluid. Mech.* **220**, 569–594.

BREUER, K. S. & LANDAHL, M. T. 1990 The evolution of a localized disturbance in a laminar boundary layer. Part 2. Strong disturbances. *J. Fluid Mech.* **220**, 595–621.

BULLISTER, E. T. & ORSZAG, S. A. 1987 Numerical simulation of turbulent spots in channel and boundary layer flows. *J. Sci. Comput.* **2**, 263–281.

BUTLER, K. M. & FARRELL, B. F. 1992 Three-dimensional optimal perturbations in viscous shear flow. *Phys. Fluids* A **4**, 1637–1650.

CHAMBERS, F. W. & THOMAS, A. S. W. 1983 Turbulent spots, wave packets and growth. *Phys. Fluids* **26**, 1160–1162.

COHEN, J., BREUER, K. S. & HARITONIDIS, J. H. 1991 On the evolution of a wave packet in a laminar boundary layer. *J. Fluid Mech.* **225**, 575–606.

DIPRIMA, R. C. & HABETLER, G. J. 1969 A completeness theorem for non-selfadjoint eigenvalue problems in hydrodynamic stability. *Arch. Rat. Mech. Anal.* **32**, 218–227.

DRAZIN, P. G. & REID, W. H. 1981 *Hydrodynamic Stability*. Cambridge University Press.

ECKHAUS, W. 1965 *Studies in Non-linear Stability*. Springer.

ELLINGSEN, T. & PALM, E. 1975 Stability of linear flow. *Phys. Fluids.* **18**, 487–488.

FARRELL, B. F. 1988 Optimal excitation of perturbations in viscous shear flow. *Phys. Fluids* **31**, 2093–2102.

FASEL, H., RIST, U. & KONZELMANN, U. 1990 Numerical investigation of the three-dimensional development in boundary layer transition. *AIAA J.* **28**, 29–37.

GILBERT, N. 1988 Numerische Simulation der Transition von der laminaren in die turbulente Kanalströmung. *Tech. Rep.* DFVLR-FB 88-55, DFVLR, Göttingen, Germany.

GILBERT, N. & KLEISER, L. 1990 Near-wall phenomena in transition to turbulence. In *Near-Wall Turbulence: 1988 Zoran Zaric Mem. Conf.* (ed. S. J. Kline & N. H. Afgan), pp. 7–27. Hemisphere.

GREENGARD, L. 1988 Spectral integration and two-point boundary value problems. *Yale University, Dept Comput. Sci. Res. Rep.* YALEU/DCS/RR-646.

GUSTAVSSON, L. H. 1979 Initial value problem for boundary layer flows. *Phys. Fluids* **22**, 1602–1605.

GUSTAVSSON, L. H. 1986 Excitation of direct resonances in plane Poiseuille flow. *Stud. Appl. Maths* **75**, 227–248.

GUSTAVSSON, L. H. 1991 Energy growth of three-dimensional disturbances in plane Poiseuille flow. *J. Fluid Mech.* **224**, 241–260.

GUSTAVSSON, L. H. & HULTGREN, L. S. 1980 A resonance mechanism in plane Couette flow. *J. Fluid Mech.* **98**, 149–159.

HENNINGSON, D. S. 1988 The inviscid initial value problem for a piecewise linear mean flow. *Stud. Appl. Maths* **78**, 31–56.

HENNINGSON, D. S. 1991 An eigenfunction expansion of localized disturbances. In *Advances in Turbulence 3* (ed. A. V. Johansson & P. H. Alfredsson), pp. 162–169. Springer.

HENNINGSON, D. S., JOHANSSON, A. V. & LUNDBLADH, A. 1990 On the evolution of localized disturbances in laminar shear flows. In *Laminar–Turbulent Transition* (ed. D. Arnal & R. Michel), pp. 279–284. Springer.

HENNINGSON, D. S. & KIM, J. 1991 On turbulent spots in plane Poiseuille flow. *J. Fluid Mech.* **228**, 183–205.

HENNINGSON, D. S. & SCHMID, P. J. 1992 Vector eigenfunction expansions for plane channel flows. *Stud. Appl. Maths* **87**, 15–43.

HENNINGSON, D. S., SPALART, P. & KIM, J. 1987 Numerical simulations of turbulent spots in plane Poiseuille and boundary layer flows. *Phys. Fluids* **30**, 2914–2917.

HERBERT, T. 1988 Secondary instability of boundary layers. *Ann. Rev. Fluid Mech.* **20**, 487–526.

HULTGREN, L. S. & GUSTAVSSON, L. H. 1981 Algebraic growth of disturbances in a laminar boundary layer. *Phys. Fluids* **24**, 1000–1004.

KIM, J., MOIN, P. & MOSER, R. 1987 Turbulence statistics in fully developed channel flow. *J. Fluid Mech.* **177**, 133–166.

KIM, J. & MOSER, R. 1989 On the secondary instability in plane Poiseuille flow. *Phys. Fluids* A **1**, 775–777.

KLEBANOFF, P. S., TIDSTROM, K. D. & SARGENT, L. M. 1962 The three-dimensional nature of boundary layer instability. *J. Fluid Mech.* **12**, 1–34.

KLEISER, L. & ZANG, T. A. 1991 Numerical simulation of transition in wall-bounded shear flows. *Ann. Rev. Fluid Mech.* **23**, 495–537.

KLINGMANN, B. G. B. 1992 On transition due to three-dimensional disturbances in plane Poiseuille flow. *J. Fluid Mech.* **240**, 167–195.

KOVASZNAY, L. S. G., KOMODA, H. & VASUDEVA, B. R. 1962 Detailed flow field in transition. In *Proc. 1962 Heat Transfer and Fluid Mechanics Institute, Stanford University*, pp. 1–26.

LANDAHL, M. T. 1975 Wave breakdown and turbulence. *SIAM J. Appl. Maths* **28**, 735–756.

LANDAHL, M. T. 1980 A note on an algebraic instability of inviscid parallel shear flows. *J. Fluid Mech.* **98**, 243–251.

LUNDBLADH, A., HENNINGSON, D. S. & JOHANSSON, A. V. 1992 An efficient spectral integration method for the solution of the Navier–Stokes equations. *FFA-TN* 1992-28, Aeronautical Research Institute of Sweden, Bromma.

LUNDBLADH, A. & JOHANSSON, A. V. 1991 Direct simulation of turbulent spots in plane Couette flow. *J. Fluid Mech.* **229**, 499–516.

MACK, L. M. 1976 A numerical study of the temporal eigenvalue spectrum of the Blasius boundary layer. *J. Fluid Mech.* **73**, 497–520.

MALIK, M., ZANG, T. & HUSSAINI, M. 1985 A spectral collocation method for the Navier–Stokes equations. *J. Comput. Phys.* **61**, 64–88.

MORKOVIN, M. V. 1969 The many faces of transition. In *Viscous Drag Reduction* (ed. C. Wells). Plenum.

MURDOCK, J. 1986 Three-dimensional numerical study of boundary layer stability. *AIAA Paper* 86-0434.

ORSZAG, S. A. 1971 Accurate solution of the Orr–Sommerfeld stability equation. *J. Fluid Mech.* **50**, 689–703.

ORSZAG, S. A. & KELLS, L. C. 1980 Transition to turbulence in plane Poiseuille and plane Couette flow. *J. Fluid Mech.* **96**, 159–205.

ORSZAG, S. A. & PATERA, A. T. 1983 Secondary instability of wall-bounded shear flows. *J. Fluid Mech.* **128**, 347–385.

PRUETT, C. D. & ZANG, T. A. 1992 Direct numerical simulations of laminar breakdown in high speed axi-symmetric boundary layers. *AIAA Paper* 92-0742.

REDDY, S. C. 1991 Pseudospectra of operators and discretization matrices and an application to the method of lines. PhD thesis, Massachusetts Institute of Technology.

REDDY, S. C., SCHMID, P. J. & HENNINGSON, D. S. 1993 Pseudospectra of the Orr–Sommerfeld operator. *SIAM J. Appl. Maths* **53** (1) (to appear).

RESHOTKO, E. 1976 Boundary-layer stability and transition. *Ann. Rev. Fluid Mech.* **8**, 311–350.

RILEY, J. & GAD-EL-HAK, M. 1985 The dynamics of turbulent spots. In *Frontiers of Fluid Mechanics*, pp. 123–155. Springer.

SCHENSTED, I. V. 1961 Contribution to the theory of hydrodynamic stability. PhD thesis, University of Michigan.

SCHMID, P. J. & HENNINGSON, D. S. 1992 A new mechanism for rapid transition involving a pair of oblique waves. *Phys. Fluids* A **4**, 1986–1989.

SCHUBAUER, G. B. & SKRAMSTAD, H. F. 1947 Laminar boundary layer oscillations and the stability of laminar flow. *J. Aero. Sci.* **14**, 69–78.

SPALART, P. R. & YANG, K. 1987 Numerical study of ribbon induced transition in Blasius flow. *J. Fluid Mech.* **178**, 345–365.

SQUIRE, H. B. 1933 On the stability for three-dimensional disturbances of viscous fluid flow between parallel walls. *Proc. R. Soc. Lond.* A **142**, 621–8.

TREFETHEN, L. N. 1991 Pseudospectra of matrices. In *Proc. 14th Dundee Biennial Conf. on Numerical Analysis*.

ZANG, T. & KRIST, S. 1989 Numerical experiments on stability and transition in plane channel flow. *Theoret. Comput. Fluid Dyn.* **1**, 41–64.